

NATIONAL RADIO ASTRONOMY OBSERVATORY
Charlottesville, Virginia

ELECTRONICS DIVISION INTERNAL REPORT NO. 305

**AN ADAPTIVE INTERFERENCE CANCELING RECEIVER
FOR RADIO ASTRONOMY - THEORY**

R. Bradley, S. Wilson*, C. Barnbaum and B. Wang**

RECEIVED
NOV 27 1996
AOC LIBRARY

November 1, 1996

*University of Virginia, Electrical Engineering

**NSF REU Student

Table of Contents

1.0	Introduction	1
2.0	Background Information on Adaptive Filters	4
3.0	Fundamentals of Adaptive Interference Cancellation	7
3.1	Basic Concepts	7
3.2	Error-Performance Surface and the Wiener Filter	9
3.3	Single Reference Channel Adaptive Interference Canceler	12
3.4	The LMS Algorithm	17
3.5	Multiplier Reference Adaptive Interference Cancellation	19
3.6	The Notch Filter Phenomenon	21
3.7	Adaptive Beam Formation and Sidelobe Cancellation	22
3.8	Finite Precision Errors	24
3.9	Estimated Performance of the Adaptive Canceler	27
4.0	Simulations of a Multiple Reference Interference Canceler	28
4.1	Simulator and Platform	28
4.2	Description of Adaptive Canceler System and Input Signals	28
4.3	Overall Canceler Performance	29
4.4	Investigation #1: Performance Vs. Adaptation Step Size	33
4.5	Investigation #2: Performance Vs. Number of Reference Channels	35
4.6	Investigation #3: Performance Vs. Primary Channel Noise Power	36
4.7	Investigation #4: Performance Vs. Reference Channel Noise Power	36
5.0	Conclusions	40
	Appendix	41
	List of Symbols	50
	Bibliography	53

1.0 Introduction

An increasing amount of precious radio frequency spectrum in the VHF, UHF, and microwave bands is being utilized each year to support new commercial and military ventures. Advances in both very large scale integration (VLSI) and monolithic RF (MMIC) technology has spurred a plethora of new applications, including improved point-to-point communications, wireless computer communications, and the ever-growing popularity of inexpensive cellular telephones; all have the potential to interfere with radio astronomy observations. Furthermore, the sky is being cluttered with earth-orbiting satellites supporting direct broadcast television, global personal communications, global positioning systems, and other services. Signals from satellites even occasionally leak into the designated radio astronomy bands. The increasing congestion of the radio spectrum has made astrophysical research in radio and microwave bands more difficult to pursue.

Some radio spectral lines of astronomical interest occur outside the protected radio astronomy bands and are unobservable due to heavy interference. One example, the initial motivation behind this work, is the hyperfine transition of hydrogenated buckminsterfullerene (HC_{60}), that is predicted to fall in the 90 - 100 MHz band (Morton et al., 1993). This band, which is part of the FM broadcast band that spans 88 - 108 MHz, contains FM channels that are spaced 200 kHz apart, and even in a remote radio astronomy site such as Green Bank, WV, nearly the entire band exhibits interference, as shown in Fig. 1. These signals are frequency modulated carriers that are also influenced by propagation effects between the transmitter and the receiver; the statistics of the interference signals vary as a function of time. A glance at Fig. 1 reveals that it is impossible to observe in this band without highly effective interference excision.

Over the past several years, scientists and engineers concerned with such interference have organized special workshops and conference sessions to share ideas on ways to manage this growing problem. The more conventional approaches being discussed at these meetings include the following: 1) legislation to designate regions as radio quiet areas such as the National Radio Quiet Zone (NRQZ) around Green Bank,

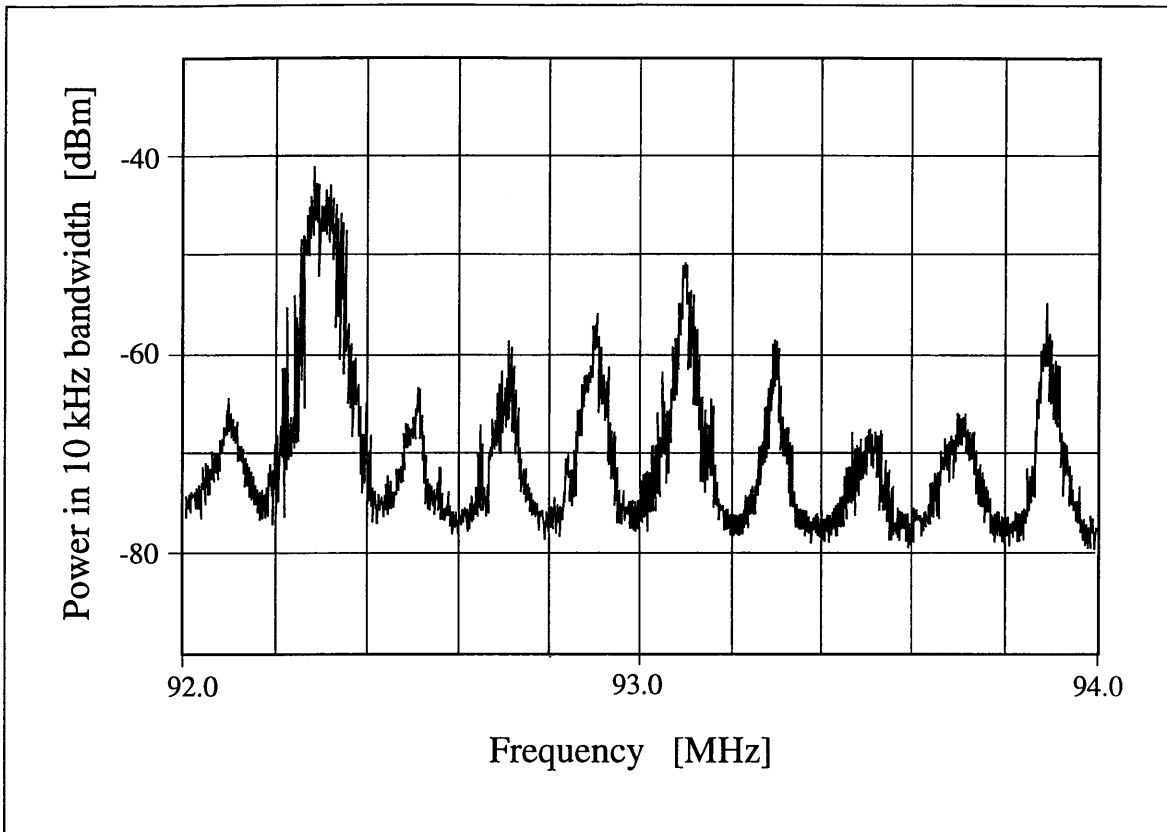


Figure 1 Spectral scan of a portion of the FM broadcast band. Data were taken on 2/13/96 using the 50-500 MHz receiver and cross-dipole feed on the 140 foot. Receiver gain was 44.5 dB and the system temperature was 750 K.

WV where the power and location of transmitters in the region are controlled (Sizemore, 1991); 2) filtering techniques such as superconducting notch filters to remove fixed-frequency interferers without substantially increasing the noise temperature of the receiver (Moffet, 1982, Superconducting Technologies, 1994); 3) blanking techniques to remove pulse-type signals from the data stream (Gerard, 1982, Fisher, 1982); 4) RF shielding to suppress spurious digital signals and local oscillator signals from adjacent electronic equipment or communication systems (Schultz, 1971); and 5) post-processing techniques such as sidelobe-beam nulling (Erickson, 1982) to remove fixed-frequency signals. All of these techniques yield some degree of interference cancellation, yet each suffers from either insufficient cancellation, inability to adapt to changing statistics of the interference signal, partial removal of wanted data, or requiring excessively large amounts of post processing on the accumulated data. Clearly, much work is needed to

investigate new approaches to interference excision that have the potential to improve upon the shortcomings of these conventional techniques.

One concept of interference excision that has not been used before in radio astronomy is adaptive interference cancellation which makes use of adaptive filters and high speed digital technology. This report, for the first time, describes the basic concept of adaptive cancellation in the context of radio astronomy instrumentation and estimates the canceler effectiveness on several radio telescopes. The results of system simulations based on FM broadcast signals as interferers is also presented. The report concludes with a summary of the important issues to consider when attempting to use this approach in radio astronomy applications.

2.0 Background Information on Adaptive Filters

The objective of the linear filtering problem is to design a linear filter with the interference data as input in order to minimize the effects of interference at the filter output according to some statistical criterion. A useful approach is to minimize the mean-square value of the error signal defined as the difference between some desired response and the actual filter output. For stationary inputs (a process is said to be stationary when the statistical characteristics of the sample functions do not change with time), the resulting solution is said to be optimum in a least-squares sense, and is commonly known as the Wiener filter. A plot of the mean-square value of the error signal versus the adjustable parameters is the error-performance surface, and the unique minimum point on the surface is the Wiener solution. However, the Wiener solution is inadequate for dealing with non-stationary conditions of the interference signal where the orientation of the error-performance surface will vary as a function of time. The Wiener solution is non-adaptive and to make use of it requires *a priori* information about the statistics of the data being processed.

The adaptive filter is self-defining by way of a recursive algorithm making it possible to perform satisfactorily in a non-stationary environment. The algorithm starts at an initial set of conditions, and in a stationary environment, will converge to the optimal Wiener solution in some statistical sense. In a non-stationary environment the algorithm offers a tracking capability (i.e., can track the variations in the statistics of the input data) provided that the variations are sufficiently slow. Note that in the adaptive filter, the filter parameters become data dependent, which is characteristic of a nonlinear device that does not obey the principle of superposition. However, it is classified as linear in the sense that the estimate of the quantity of interest is computed adaptively as a linear combination of the available observations applied to the filter input.

The applications of adaptive filters can be classified into four categories (Haykin, 1996): 1) Identification, in which a linear model is adapted to represent the best fit to an unknown time-varying process, where the process and the filter are driven by the same input; 2) Inverse Modeling, in which the adaptive filter provides the inverse model to represent the unknown process so that the inverse model ideally has a transfer function

that is equal to the reciprocal of the unknown process; 3) Prediction, in which the adaptive filter provides the best prediction of the present value of a random signal, where the actual present value is the desired response; and 4) Interference Canceling, in which the adaptive filter is used to cancel unknown interference contained alongside the information bearing signal component in the primary channel, with the cancellation being optimized in some sense. It is in this latter category that the adaptive filter will be used in the context of radio astronomy interference excision.

Early work on adaptive interference cancellation was limited to narrow audio bandwidths. Around 1965, an adaptive echo canceler for telephone lines was developed at Bell Telephone Laboratories (Sondhi, 1967). Also in 1965, an adaptive line enhancer (ALE) was built to cancel 60 Hz interference at the output of an electrocardiographic (ECG) amplifier and recorder (Widrow et al., 1975). In 1972, a group of students at Stanford University used adaptive filtering to cancel the maternal ECG in fetal electrocardiography, where the mother's heartbeat has an amplitude from two to ten times stronger than the fetal heartbeat (Widrow et al., 1975). Over the past twenty years, such audio interference cancellation systems have been developed for many diverse applications from speech enhancement for communications in noisy environments to the reduction of harmful noise in harsh work environments. There is even a company, Noise Cancellation Technologies Corporation, that specializes in noise reducing audio systems for portable radio telephone applications (Goldberg, 1995)!

Extending the adaptive filtering concept to wideband applications above a few hundred kilohertz has required advances in the digital hardware. Operation up to a few megahertz can now be performed using modern digital signal processing chips such as the Logic Devices Inc. LMA1009 12 x 12 bit multiplier-accumulator chip (Logic Devices, 1995). The development of the Acoustic Charge Transport (ACT) programmable transversal filter (Fleisch et al., 1991) permits limited precision operation up to about 100 MHz. Bullock (1990) describes a wideband adaptive filter which uses the ACT to remove narrowband interference. The system input, which contains both the desired (wideband) and reference (narrowband) signals, is processed by a decorrelation delay that separates the two components (Widrow et al., 1975). The adaptive filter is then used to suppress

the narrowband signal. With this technique, suppression up to 30 dB was demonstrated. Lin et al. (1992) describe an Interference Cancellation System based on the ACT for electronic warfare applications. This system uses a two step cross correlation process that identifies the frequency and time delay of the interference and then engages an adaptive filter to yield over 40 dB of interference suppression on AM and FM signals. This suppression is limited by the precision (number of bits) used for controlling the ACT. Future improvements in the state-of-the-art will require further advances in ACT or related technologies.

Closely related to adaptive interference cancellation in the temporal domain is adaptive beam formation in the spatial domain for applications such as antenna sidelobe cancellation. The basic sidelobe canceler uses a primary (high-gain) antenna and a reference omni-directional (low-gain) antenna to form the a two-element array with one degree of freedom that makes it possible to steer a deep null in the sidelobe region of the combined antenna pattern. In particular, the null is placed in the direction of the interferer, with only minor perturbations of the main lobe (Howells, 1976). A complete description of adaptive antenna systems is found in Widrow (1967).

The sidelobe canceler is similar to the radio telescope array described by Erickson (1982), who has shown that a single interferer can be reduced to the noise level by post-processing the data with an algorithm that first identifies a beam in the direction of the interference and then uses this beam to form a null in the array pattern. The primary difference between Erickson's approach and the adaptive system is that the adaptive filter performs the cancellation in real time and therefore requires no post processing. Furthermore, the adaptive filter can track changes in the interference while the post processing scheme assumes that the characteristics of the interference are quasi-stationary. The adaptive system analyzed in this report operates in the time domain, but as will be shown, the overall effect on the telescope is to reduce the interference through both temporal and spatial cancellation.

3.0 Fundamentals of Adaptive Interference Cancellation

In this section, we present the theory of adaptive interference cancellation. For a more complete description, see Widrow et al. (1985). The section begins with a look at the overall system concept and then we describe the performance of the system for a single channel adaptive interference canceler in the presence of stationary inputs (Wiener solution). Next, we describe the algorithm for the adaption process. The basic concept is then extended to include multiple reference inputs, and we compare this system with adaptive beamforming. This section closes with a brief note on finite precision errors and an estimate of canceler performance on several radio telescopes.

3.1 Basic Concepts

An ideal adaptive interference canceling system for use on a radio telescope is depicted in Fig. 2. All of the signals are digitized with a constant sampling period, giving rise to discrete time sequences indexed by n . The telescope receiver, located at the prime focus, forms the primary input to the canceler. This input consists of the desired astronomical signal, $s(n)$, entering through the main beam, as well as undesired interference, $i_p(n)$, entering through the telescope sidelobes. We assume here that the power density of the interference will preclude astronomical observing, but will not be strong enough to "overload" the receiver (overloading occurs when the amplitude of the signal causes the amplifiers to operate outside of their linear range, resulting in the generation of spurious signals). A second receiver connected to an omni-directional antenna forms the reference input, $x(n)$, to the canceler. This input consists of only the interference, $i_x(n)$, which is uncorrelated with the astronomical signal, but correlated in some unknown way with the interference in the primary channel. Here we assume that the desired astronomical signal does not contribute to the reference input. In the reference channel, the interference is filtered to produce the output, $y(n)$, that is a close replica to $i_p(n)$. This filter output is subtracted from the primary input, $s(n) + i_p(n)$, to produce the system output, $\varepsilon(n)$. It is important to note that no prior knowledge of $s(n)$, $i_p(n)$, or $i_x(n)$ or their interrelationships, either statistical or deterministic, is required.

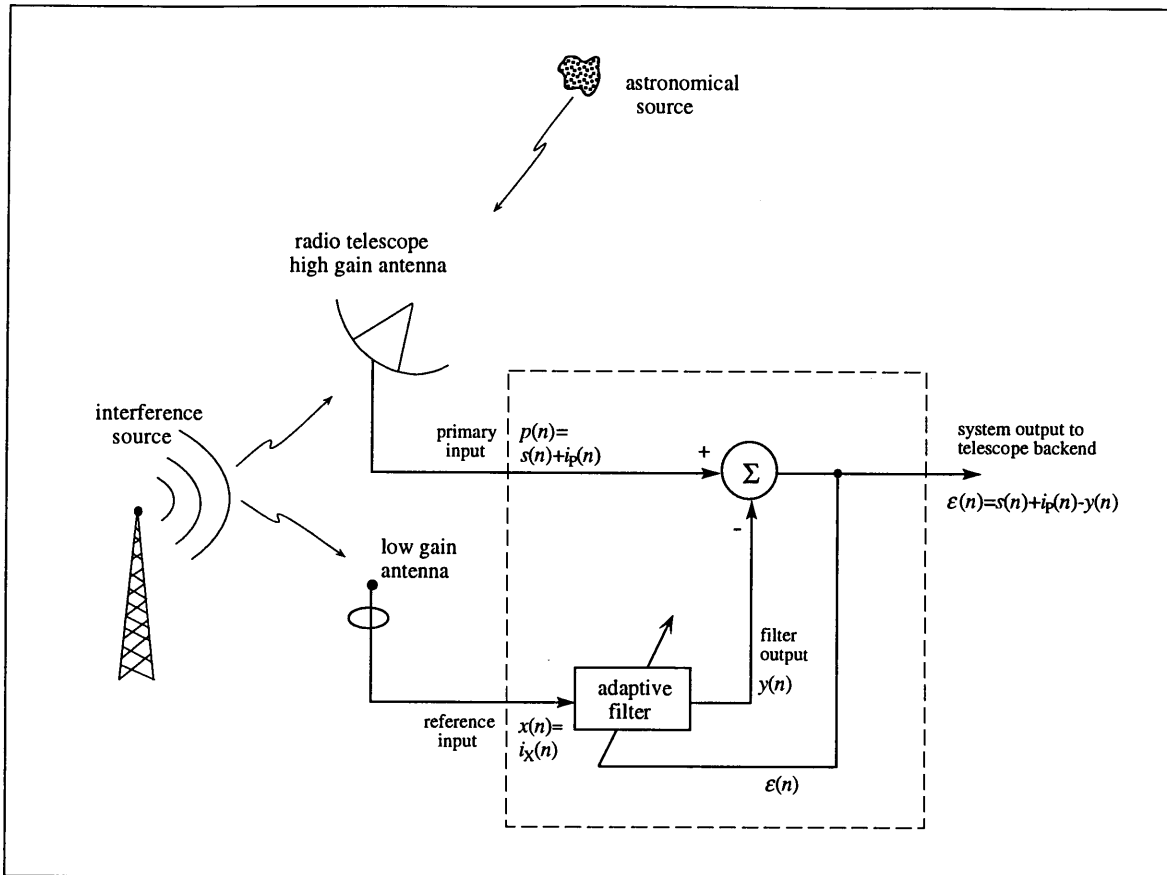


Figure 2 The fundamental concept of adaptive interference cancellation as applied to a single dish radio telescope.

Fixed filters are inapplicable in dynamic interference canceling situations because the correlation and cross-correlation functions of the primary and reference inputs are generally unknown and often variable with time. Adaptive filters are required to "learn" the statistics initially and then to track them if they vary slowly. However, under slowly-varying non-stationary conditions, the steady-state performance of adaptive filters closely approximates that of fixed optimal filters, and therefore Wiener filter theory provides a convenient mathematical analysis of statistical interference canceling problems.

Based on the above argument, assume for the moment that $s(n)$, $i_p(n)$, $i_x(n)$, and $y(n)$ are statistically stationary and have zero means. Squaring the system output gives,

$$\epsilon(n)^2 = s(n)^2 + (i_p(n) - y(n))^2 + 2s(n)(i_p(n) - y(n)) \quad (1)$$

Taking expectations of both sides and noting that $s(n)$ is uncorrelated with $i_p(n)$ and $y(n)$, yields

$$E[\epsilon(n)^2] = E[s(n)^2] + E[(i_p(n) - y(n))^2] \quad (2)$$

The total signal power, $E[s(n)^2]$, will be unaffected as the filter is adjusted to minimize $E[\epsilon(n)^2]$. The minimum total output power is therefore

$$E_{\min}[\epsilon(n)^2] = E[s(n)^2] + E_{\min}[(i_p(n) - y(n))^2] \quad (3)$$

When the filter is adjusted so that $E[\epsilon(n)^2]$ is minimized, $E[(i_p(n) - y(n))^2]$ is therefore also minimized. The filter output, $y(n)$, is a best least-squares estimate of the primary interference $i_p(n)$. Hence, *minimizing the total output power minimizes the output interference power*, and since the signal in the output remains constant, minimizing the total output power maximizes the output signal-to-interference ratio (SIR).

Two special cases are worth noting. From (3), the smallest possible output power is $E[s(n)^2]$ when $E[(i_p(n) - y(n))^2] = 0$. In this case, minimizing the output power causes the output signal to be perfectly free of interference. Now consider the case when the reference input is completely uncorrelated with the interference in the primary input. The filter will turn itself off and will not increase output power. In this case, $y(n)$ is uncorrelated with the primary input so that

$$E[\epsilon(n)^2] = E[(s(n) + i_p(n))^2] + E[y(n)^2] \quad (4)$$

Maximizing the output power requires that $E[y(n)^2]$ be minimized, which is accomplished by making the filter coefficients zero, bringing $E[y(n)^2]$ to zero.

3.2 Error-Performance Surface and the Wiener Filter

Figure 3 shows the classic single-input, single-output Wiener filter, constructed using a transversal filter (also known as a tapped-delay line), and a linear combiner. The transversal filter is used in almost all interference canceling applications since it has a

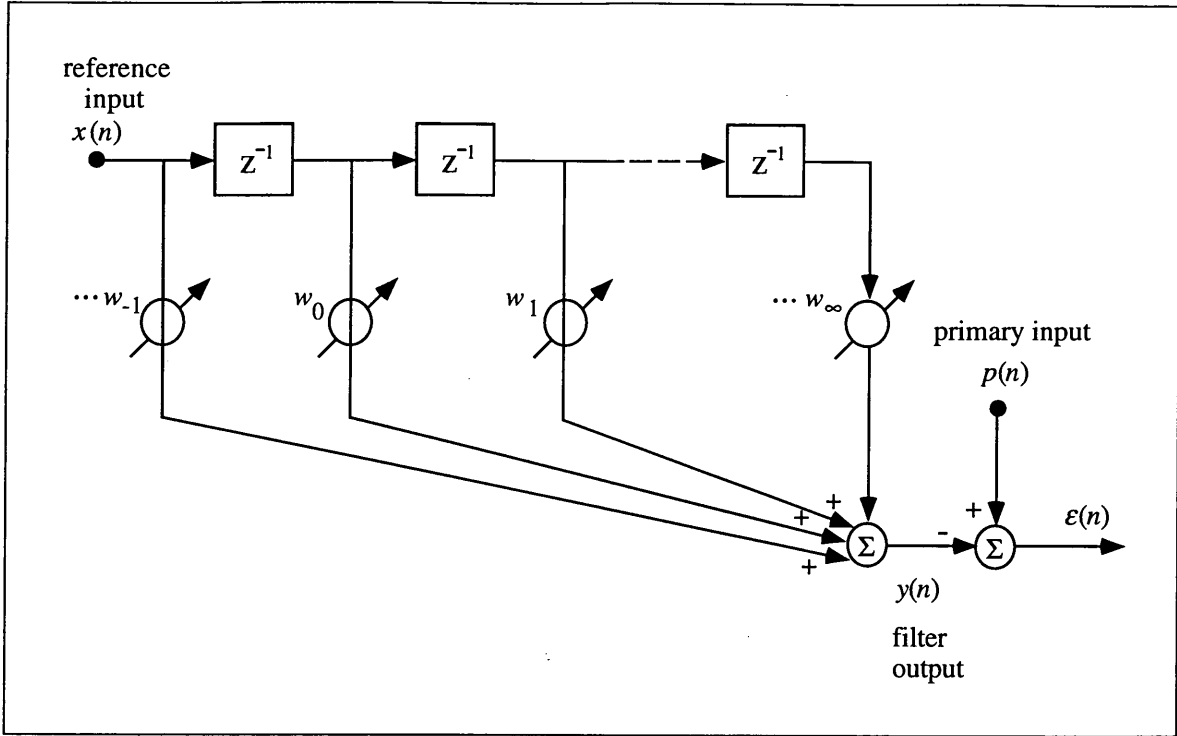


Figure 3 The Wiener filter consisting of an infinitely long tapped delay line. The filter tap weights, w_i are adjusted to yield optimal filter performance (Wiener solution) for the case of stationary processes.

finite impulse response (i.e FIR-type filter) making it inherently stable. The unit delay, z^{-1} , is one sample time in duration. The system output, $\varepsilon(n)$, (also known as the error signal) is equal to the difference between the primary input, $p(n) = s(n) + i_p(n)$, and the inner product of the vector $X(n)$ formed by the delayed versions of $x(n)$, and the filter tap weight vector, $W(n)$,

$$\varepsilon(n) = p(n) - X(n)^T W(n) \quad (5)$$

where T indicates transposition. The instantaneous squared error becomes

$$\varepsilon(n)^2 = p(n)^2 + W(n)^T X(n) X(n)^T W(n) - 2 p(n) X(n)^T W(n) \quad (6)$$

Assume for the moment that $\varepsilon(n)$, $p(n)$, and $X(n)$ are statistically stationary. Taking the expected value over n yields the mean-square error function,

$$E[\epsilon(n)^2] = E[p(n)^2] + \mathbf{W}(n)^T E[\mathbf{X}(n)\mathbf{X}(n)^T] \mathbf{W}(n) - 2E[p(n)\mathbf{X}(n)^T] \mathbf{W}(n) \quad (7)$$

The signals $x(n)$ and $p(n)$ are not generally independent. The elements that make up (7) are all constant second-order statistics when the vector $\mathbf{X}(n)$ and $p(n)$ are stationary, so the error performance surface, $\xi = E[\epsilon(n)^2]$, defined by (7) is quadratic, forming a hyperparaboloid that is concave upward and therefore has a unique minimum. Knowing that the correlation function, ϕ , is equivalent to the expected value function for a stationary process, and expanding the matrix operations, the error performance surface becomes

$$\xi = \phi_{PP}(0) + \sum_{l=-\infty}^{\infty} \sum_{m=-\infty}^{\infty} w(n)_l w(n)_m \phi_{XX}(l-m) - 2 \sum_{l=-\infty}^{\infty} w(n)_l \phi_{XP}(-l) \quad (8)$$

which is constant for stationary processes.

The minimum point on this surface corresponds to the optimum weight vector, \mathbf{W}_{opt} . The values of \mathbf{W}_{opt} can be found by setting the derivatives of ξ with respect to the weights equal to zero. Thus

$$\frac{\partial \xi}{\partial w(n)} = 2 \sum_{l=-\infty}^{\infty} w(n)_l \phi_{XX}(n-l) - 2 \phi_{XP}(-n) = 0 \quad (9)$$

and therefore the Wiener-Hopf equation is obtained,

$$\sum_{l=-\infty}^{\infty} w_{opt\ l} \phi_{XX}(n-l) = \phi_{XP}(n) \quad (10)$$

Taking the z transform of (10), the convolution on the left side becomes a product and, defining $W_{opt}(z) = z$ transform of $[w_{opt}(n)]$,

$$W_{opt}(z) = \frac{\Phi_{XP}(z)}{\Phi_{XX}(z)} \quad (11)$$

The z transform of the optimum impulse response is the ratio of the cross power spectrum between the input to the transversal filter, $x(n)$, and the primary input, $p(n)$, to the power spectrum of $x(n)$. This result represents the unconstrained, noncausal

solution to the Wiener filtering problem. Refer to (Oppenheim et al., 1989) for details of the z-domain and z transforms.

The practical adaptive filter, having a finite number of filter taps, can closely approximate the system described above. The typical impulse response of ideal filters approach amplitudes of zero exponentially with time, and so an FIR filter can be used successfully. The more weights used in the filter, the closer the impulse response will be to the ideal (infinitely long) filter. However, increasing the number of tap weights also increases the cost of implementation and may not even be required in many applications. A practical filter size was chosen for use in the simulations.

To be physically realizable, the system must be causal. In order for the physical system to approach the performance of the ideal two-sided noncausal filter, *a delay must be inserted in the primary input*. This delay causes an equal delay to develop in the response of the filter. The length of this delay is chosen to cause the peak of the impulse response to be centered along the tapped-delay line.

3.3 Single Reference Channel Adaptive Interference Canceler

We will use the linear model outlined in Fig. 4 to analyze the performance of the single reference channel adaptive interference canceler shown in Fig. 2. This analysis neglects any nonlinear time-varying effects caused by the adaptation algorithm. The model includes the transfer function $H(z)$, which describes the characteristics of the propagation path for the interference between the source, ψ_1 , and the reference channel input. $H(z)$ is defined relative to the interference path from source to the primary channel which has been normalized to unity. The interference arriving at the reference input, $i_x(n)$, results from ψ_1 convolved with the impulse response of this path, $h(n)$. For simplicity, we have assumed that both $i_p(n)$ and $i_x(n)$ have the same spatial polarization. The model also includes the noise temperatures for the primary and reference receivers, $T_{sys P}$ and $T_{sys X}$, yielding the uncorrelated noise components $m_p(n)$ and $m_x(n)$ respectively. Conversely, $i_p(n)$ and $i_x(n)$ have the same origin and so are correlated with each other, yet uncorrelated with $s(n)$, $m_p(n)$, or $m_x(n)$. All components are assumed to have a finite power spectra at all frequencies.

The reference input to the canceler is $m_x(n) + i_x(n)$. The primary input, is $s(n) + m_p(n) + i_p(n)$. The error signal, $\epsilon(n)$, is the canceler output. Assuming that the adaptive filter has converged, and the minimum-mean-square-error solution has been found, the adaptive filter is equivalent to the Wiener filter discussed in the previous section. The optimal unconstrained transfer function, $W_{opt}(z)$ of the filter can be found from the power spectra ratio of (11). The spectrum of the filter input, $\Phi_{xx}(z)$, can be expressed in terms of the spectra of two mutually uncorrelated additive components, the spectrum of the

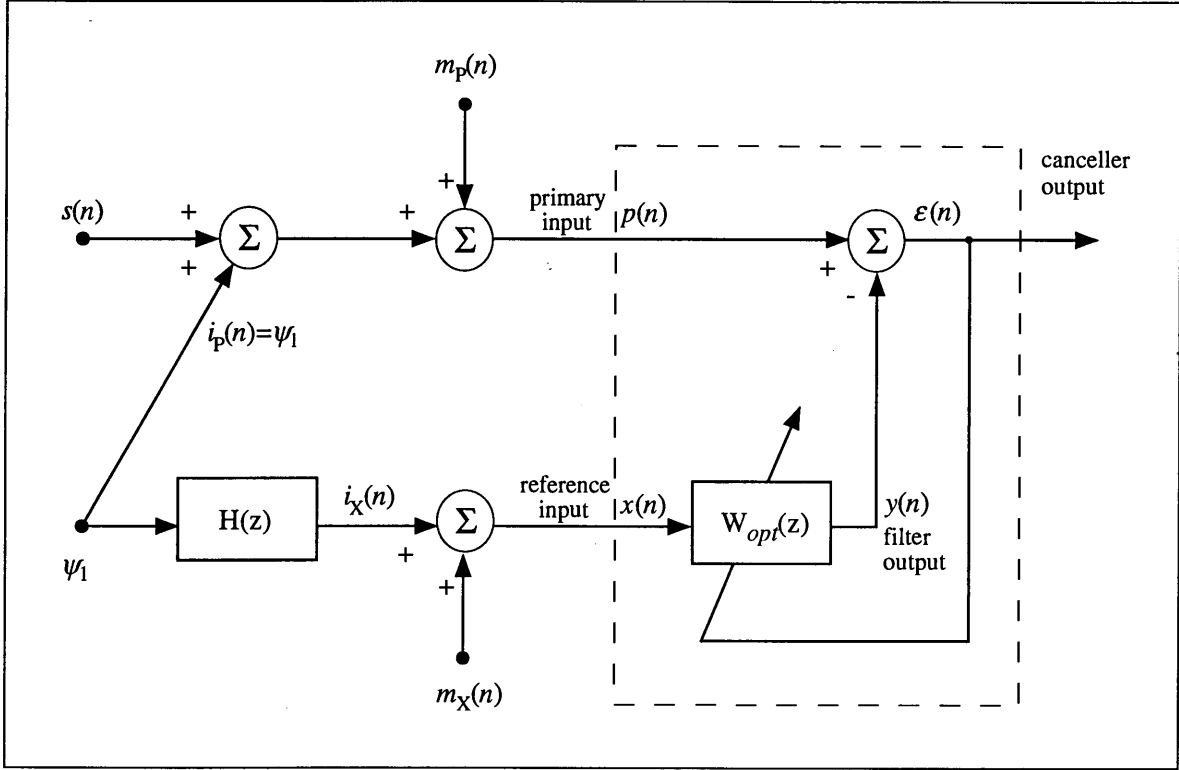


Figure 4 Model of the system shown in Fig. 2. The model includes the noise temperatures of the primary and reference receivers and the channel transfer functions for the interference paths.

noise $m_x(n)$ and that of the interference $\psi_1 = i_p(n)$ arriving via $H(z)$,

$$\Phi_{xx}(z) = \Phi_{m_x m_x}(z) + \Phi_{i_p i_p}(z) |H(z)|^2 \quad (12)$$

The cross power spectrum between the reference input and the primary input depends only on the mutually correlated components, and is given by

$$\Phi_{xP}(z) = \Phi_{i_p i_p}(z) H^*(z) \quad (13)$$

where * denotes the complex conjugate. From (11), (12), and (13), the filter transfer function becomes

$$W_{opt}(z) = \frac{\Phi_{i_p i_p}(z) H^*(z)}{\Phi_{m_x m_x}(z) + \Phi_{i_p i_p}(z) |H(z)|^2} \quad (14)$$

Note that $W_{opt}(z)$ is independent of the primary spectrum $\Phi_{ss}(z)$ and of the primary system noise spectrum $\Phi_{m_p m_p}(z)$.

The performance of the single-channel canceler can be evaluated in terms of two quantities: the *interference attenuation* (IA), and the *residual noise ratio* (RNR). To calculate these quantities, the channel interference-to-noise ratios were defined as

$$INR_{pri}(z) \doteq \frac{\Phi_{i_p i_p}(z)}{\Phi_{m_p m_p}(z)} \quad (15)$$

$$INR_{ref}(z) \doteq \frac{\Phi_{i_p i_p}(z) |H(z)|^2}{\Phi_{m_x m_x}(z)} \quad (16)$$

Using these definitions, the optimal filter transfer function (14) becomes

$$W_{opt}(z) = \frac{INR_{ref}(z)}{H(z)[INR_{ref}(z) + 1]} \quad (17)$$

The interference attenuation is defined as the ratio of the interference power spectrum at the canceler output, $\Phi_{i_o i_o}(z)$, to the interference power spectrum at the primary channel input, $\Phi_{i_p i_p}(z)$,

$$\frac{\Phi_{i_o i_o}(z)}{\Phi_{i_p i_p}(z)} = [1 - H(z)W_{opt}(z)]^2 \quad (18)$$

which results from the propagation of $i_p(n)$ through two paths, one via the primary channel and the other through the reference channel. Substitution of equation (17) into (18) gives the interference attenuation as

$$IA(z) = [INR_{ref}(z) + 1]^2 \quad (19)$$

A plot of the interference attenuation as a function of $INR_{ref}(z)$ is shown in Fig. 5. The magnitude of the attenuation for moderate values of $INR_{ref}(z)$ can be quite substantial since it is proportional to the square of the reference channel INR. Note that the interference attenuation is frequency dependent, since all quantities are a function z .

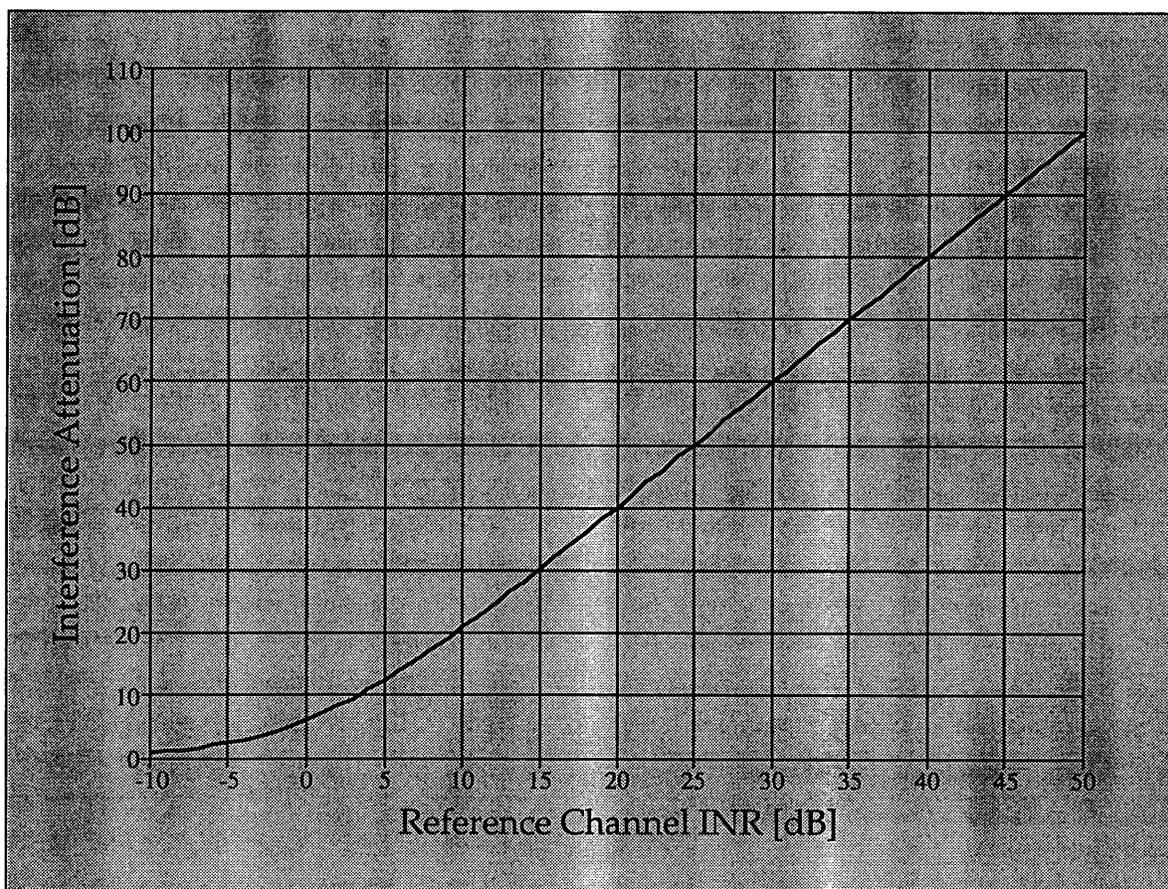


Figure 5 Graph of the Interference Attenuation (IA) as a function of reference channel INR.

Because the reference channel noise is not zero, some noise will be added to the output of the canceler. The residual noise ratio, which provides a measure of this noise

component, is defined as the ratio of the noise power spectrum at the canceler output to the noise power spectrum at the primary channel input,

$$RNR(z) = \frac{\Phi_{m_p m_p}(z) + \Phi_{m_x m_x}(z) W_{opt}(z)^2}{\Phi_{m_p m_p}(z)} \quad (20)$$

resulting from a portion of the noise present in the reference channel added to the noise in the primary channel. Substitution of equations (15), (16), and (17) into (20) yields the desired form of $RNR(z)$,

$$RNR(z) = \frac{INR_{ref}(z) INR_{pri}(z)}{[INR_{ref}(z) + 1]^2} + 1 \quad (21)$$

where the residual noise ratio is also frequency dependent. A plot of $RNR(z)$ as a function of the primary channel INR for several values of $INR_{ref}(z)$ relative to $INR_{pri}(z)$ is given in Fig. 6. If $INR_{ref}(z) = INR_{pri}(z)$, the noise power spectrum at the canceler output can be as high as twice that of the primary channel input for large values of $INR_{pri}(z)$. However, as the $INR_{ref}(z)$ increases relative to $INR_{pri}(z)$, the amount of noise added by the canceler drops to a maximum of 10 percent for 10 dB, 3.2 percent for 15 dB, and 1 percent for 20 dB. As INR_{ref} approaches infinity, the residual noise ratio approaches unity. *Therefore, a large value for $INR_{ref}(z)$ relative to $INR_{pri}(z)$ is essential in order to minimize the amount of noise added by the canceler. A large INR_{ref} will improve the interference attenuation as well.*

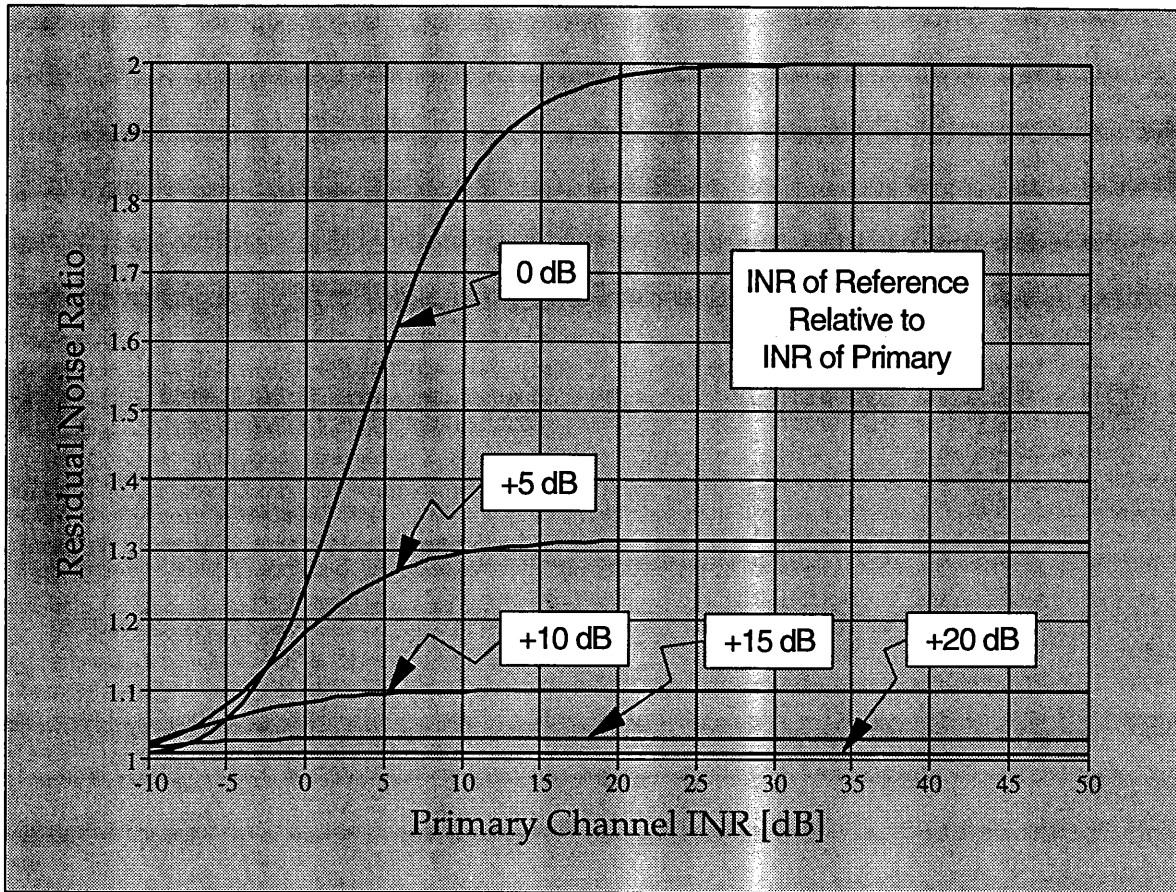


Figure 6 Graph of residual noise ratio as a function of primary channel INR for various values of reference channel INR (relative to the primary channel INR).

3.4 The LMS Algorithm

In this section, we introduce the Least-Mean-Square (LMS) algorithm for descending on the performance surface. This algorithm uses a special estimate of the gradient that is closely tied with the structure of the transversal filter. As a result, the algorithm requires a minimal amount of computing and is therefore easy to implement in hardware. There are many other algorithms offering improvements over LMS, examples include the Recursive Least-Squares (RLS) algorithm (Haykin, 1996) which requires off-line gradient estimations, and the newly proposed Higher-Order Statistics (HOS) algorithm (Shin, 1994) which uses higher (greater than 2) order cumulants to mitigate narrowband and wideband interferences but involves greater computational

complexity. However, the LMS algorithm will be used here because of its simplicity.

The derivation of the LMS algorithm presented here follows that given by Widrow et al. (1985). The transversal filter and linear combiner shown in Fig. 3 has an output given by equation (5), where again $X(n)$ is the vector of delayed versions of input samples from the reference input. The squared-error, $\epsilon(n)^2$ as given in (6), is taken as an estimate of the error performance surface, $\xi(n)$, now a function of the time index n . Then, at each iteration in the adaptive process, the gradient estimate is of the form

$$\nabla(n) = \begin{bmatrix} \frac{\partial \epsilon^2(n)}{\partial w_0(n)} \\ \vdots \\ \frac{\partial \epsilon^2(n)}{\partial w_L(n)} \end{bmatrix} = 2\epsilon(n) \begin{bmatrix} \frac{\partial \epsilon(n)}{\partial w_0(n)} \\ \vdots \\ \frac{\partial \epsilon(n)}{\partial w_L(n)} \end{bmatrix} = -2\epsilon(n)X(n) \quad (22)$$

where L is the number of filter tap weights. With this simple estimate of the gradient, the new weight vector can be calculated from the current weight vector by applying the method of gradients (also known as the method of steepest descent),

$$W(n+1) = W(n) - \mu \nabla(n) = W(n) + 2\mu \epsilon(n)X(n) \quad (23)$$

where μ is the gain constant that regulates the speed and stability of adaptation. This is the LMS algorithm.

This LMS algorithm can be implemented in a practical system without squaring, averaging, or differentiation and is elegant in its simplicity and efficiency. Without averaging, the gradient components contain a large component of noise, but the noise is attenuated with time by the adaptive process which acts as a low-pass filter in this respect. Convergence criteria for the weight vector mean toward the optimum weight vector, place bounds on μ , but within these bounds the speed of adaptation and the noise in the weight vector solution are determined by the size of μ . It can be shown (Widrow et al., 1985) that the convergence of the weight vector mean is assured when

$$0 < \mu < \frac{1}{(L+1)(E[x^2(n)])} \quad (24)$$

Since $E[x^2(n)]$ is the reference signal power, the optimum value of μ for best convergence is anticipated to be a function of interference power. We explore this in the simulations.

Another important issue in adaptive filters is the misadjustment, M_{ADJ} , which is defined as the ratio of the excess mean-square error to the minimum mean-square error, and is a measure of how closely the adaptive process tracks the true Wiener solution. It can be shown (Widrow et al., 1985) that the misadjustment for the LMS process is

$$M_{ADJ} \approx \mu \operatorname{tr}(E[X(n)X^T(n)]) = \mu \operatorname{tr}[R(n)] \quad (25)$$

where tr indicates the trace operation on the *input correlation matrix*, $R(n) = E[X(n)X^T(n)]$. There is a trade-off between misadjustment and rate of adaptation, i.e, a smaller value of μ gives a smaller misadjustment, but the algorithm will take much longer to converge. Again, we explore this trade-off in the simulations.

3.5 Multiple Reference Adaptive Interference Canceling

When more than one interference signal must be canceled, the single reference channel adaptive system lacks the necessary degrees of freedom to eliminate both signals adequately, and so the result is far from optimum. The effectiveness of the cancellation can be improved substantially by increasing the number of adaptive filter reference inputs to equal or exceed the anticipated number of interference signals that are likely to be encountered. The reference inputs could also include orthogonal spatially-polarized elements. A model of the multiple reference system is shown in Fig. 7 (Widrow et al., 1975). This model shows M mutually uncorrelated sources of interference, ψ_1 through ψ_M . The transfer functions, $G_i(z)$ represent the propagation paths from these sources to the primary inputs. The transfer functions, $F_{ij}(z)$ similarly represent the propagation paths to the reference inputs and allow for cross-coupling.

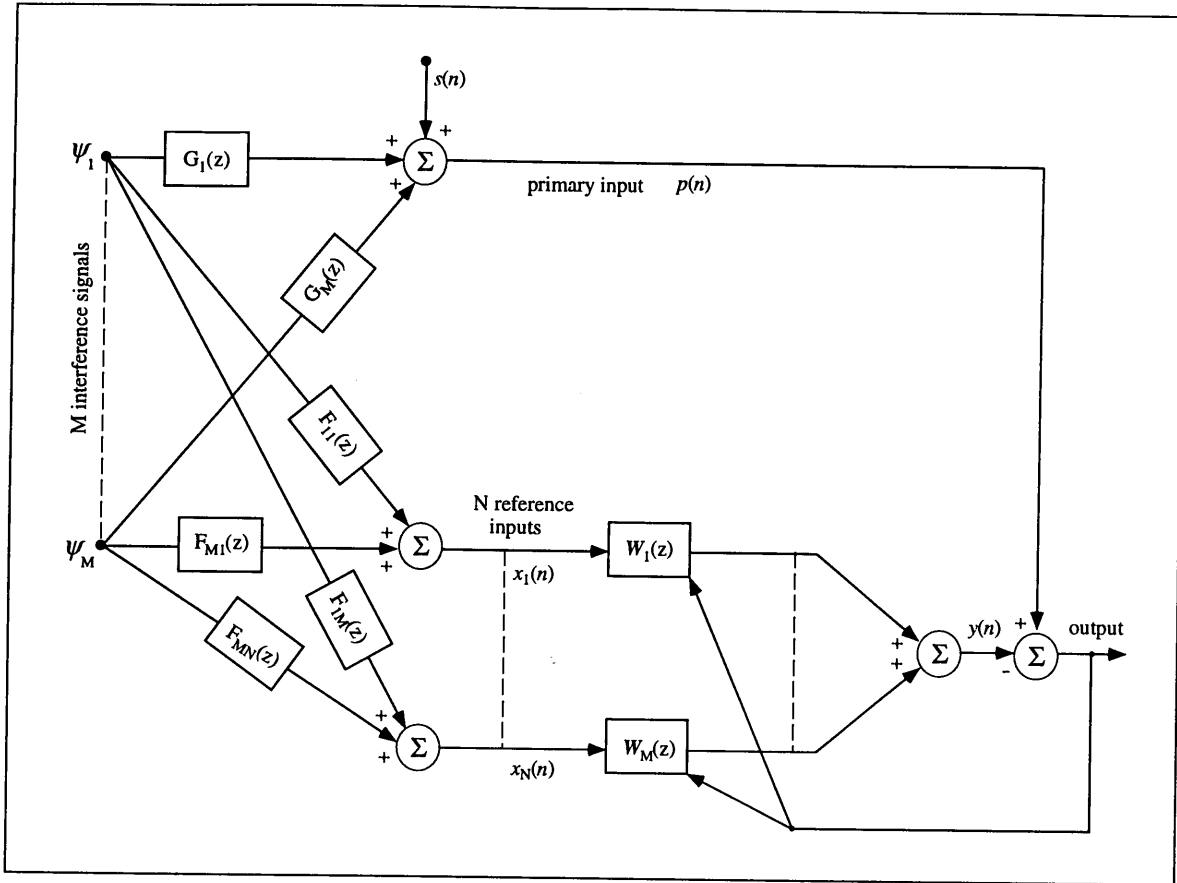


Figure 7 Model of a multiple reference channel adaptive interference canceler. There are M mutually uncorrelated interference sources and N reference inputs.

The optimal unconstrained transfer function for the filter weights is a matrix analogous to (11) and is derived as follows. The interference source spectral matrix is defined as

$$[\Phi_{\psi\psi}(z)] = \begin{bmatrix} \Phi_{\psi_1\psi_1}(z) & & & & 0 \\ & \Phi_{\psi_2\psi_2}(z) & & & \\ & & \ddots & & \\ & & & \ddots & \\ 0 & & & & \Phi_{\psi_M\psi_M}(z) \end{bmatrix} \quad (26)$$

The spectral matrix of the N reference channels becomes

$$[\Phi_{XX}(z)] = [F(z^*)]^T [\Phi_{\psi\psi}(z)] [F(z)] \quad (27)$$

where

$$[F(z)] = \begin{bmatrix} F_{11}(z) & \dots & F_{1N}(z) \\ \vdots & & \vdots \\ F_{M1}(z) & \dots & F_{MN}(z) \end{bmatrix} \quad (28)$$

The cross-spectral vector from the reference inputs to the primary input is given by

$$[\Phi_{XP}(z)] = [F(z^*)]^T [\Phi_{\psi\psi}(z)] G(z) \quad (29)$$

From (27) and (29), the set of optimal weight vectors, $W_{opt\ 1}$ through $W_{opt\ N}$ becomes the matrix

$$\begin{aligned} [W_{opt}(z)] &= [\Phi_{XX}(z)]^{-1} \Phi_{XP}(z) \\ &= [[F(z^*)]^T [\Phi_{\psi\psi}(z)] [F(z)]^{-1} [F(z^*)]^T [\Phi_{\psi\psi}(z)] [G(z)] \end{aligned} \quad (30)$$

Equation (30) can be used to derive steady-state optimal solutions to the multiple-interference, multiple-reference canceler. We explore the performance as a function of the number of reference channels in the simulations.

3.6 The Notch Filter Phenomenon

An interesting phenomenon will occur in the behavior of the adaptive filter if the reference channel encounters a narrow bandwidth RF carrier (approaching a sinusoid) and if a 90 degree phase shift occurs between two filter tap weights of a single transversal filter or between two channels of a multiple reference canceler system. When presented with this configuration, the canceler behaves like a high-Q notch filter. It can be shown (Widrow et al., 1975) that the poles and zeros of the filter transfer function have almost the same angle and are separated by a distance of approximately μA^2 , where μ is the step size and A is the amplitude of the sinusoid. The bandwidth, B_{notch} of the

notch is

$$B_{notch} = 2\mu A^2 \quad (31)$$

The notch filter, in response to the fixed frequency cosine waveform present in the reference channel, will cause cancellation of all primary channel input components at the reference frequency as well as at adjacent frequencies. Thus, under these circumstances, the desired primary input component may be partially canceled or distorted even though the reference input is uncorrelated with them. In practice, this kind of cancellation is of concern only when the adaptive process is rapid (large value of μ). When the adaptation is slow, the weights converge to values that are nearly fixed and the notch-type cancellation is not significant. We explore the characteristics of the notch phenomenon in the simulations.

3.7 Adaptive Beam Formation and Sidelobe Cancellation

In this section, we compare qualitatively adaptive beam formation, sidelobe cancellation, and temporal adaptive interference cancellation as applied to a radio telescope. Figure 8 shows a block diagram for the most basic type of beam former (Haykin, 1996, Widrow et al, 1967). The signals from five omni-directional antennas (which form a spatial array) are weighted (both in amplitude and in phase) and then summed together to produce the system output. The steering vector will adjust the weights to form and move the main beam, while the adaptive algorithm will look for strong interference and attempt to place a deep null in the direction of the interference. This system is restricted to single frequency operation.

For a single dish radio telescope, the main beam, which is formed by a mechanical structure, receives the desired signal, but sidelobes of the main beam can receive interference. Figure 9 shows the basic sidelobe canceler with a primary input and an array of reference inputs. The adaptation process will identify interference (through cross-correlation) that is entering the sidelobes and will use the reference array to steer nulling beams in appropriate directions. Again, this system is limited to single frequency operation.

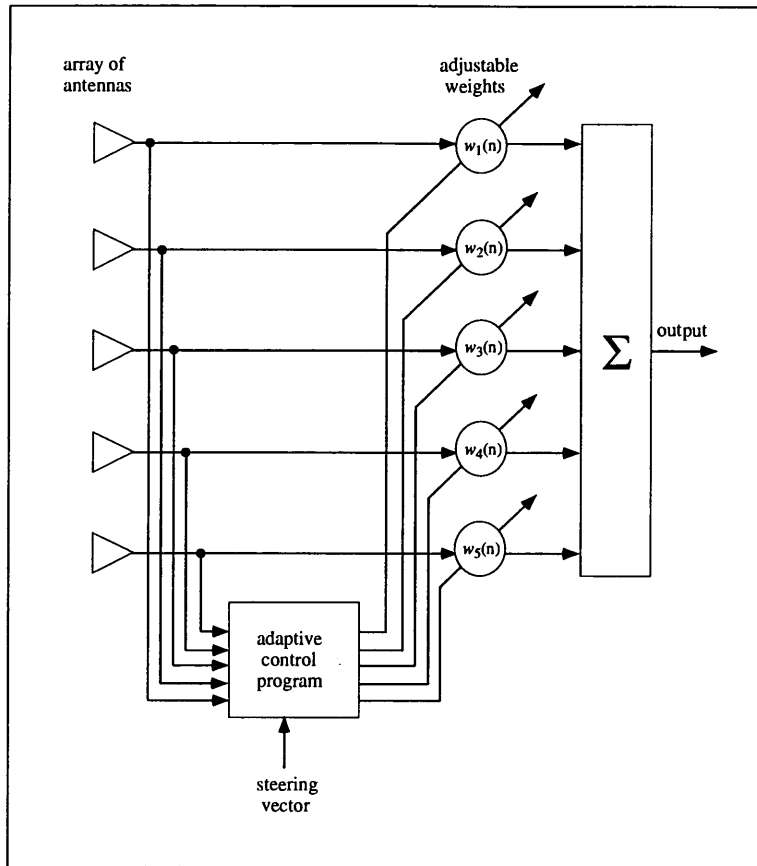


Figure 8 Block diagram of the basic adaptive beam forming system.

For wide bandwidth operation, the single complex weights must be replaced by transversal filters so that the amplitude and phase can be adjusted as desired at a number of frequencies over the band of interest. If the weight temporal spacing (delay) is sufficiently small, this network approaches the ideal filter that would allow complete control of amplitude and phase over the entire passband. Figure 10 shows the a block diagram of the adaptive canceling system which now performs both spatial and temporal canceling. This system is identical to the multi-channel canceler described in Section 3.5.

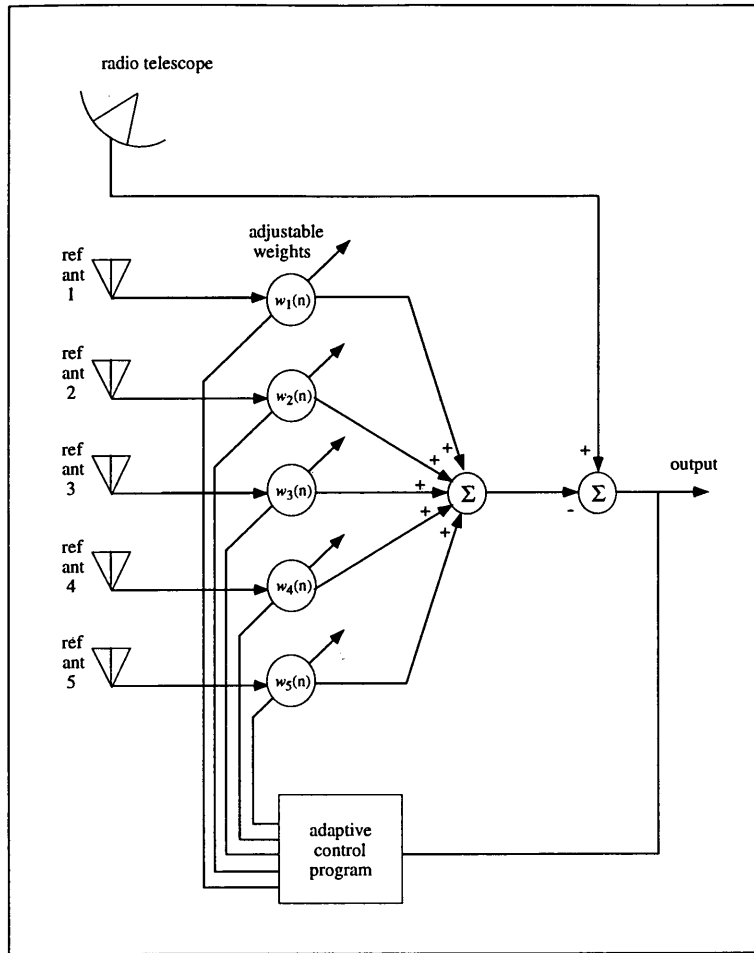


Figure 9 Block diagram of the basic sidelobe canceler system.

3.8 Finite Precision Errors

The theory of adaptive interference canceling developed in the previous sections assumes the use of infinite precision for the samples of input data as well as for the internal algorithmic calculations. This theory provides an idealized framework for the filter construction, but due to the quantization in a practical digital implementation, the performance of the filter will deviate from the theoretical value. In this section, we quote the results of an analysis on quantization effects in interference canceling systems. A complete treatment of this topic is given by Caraiscos and Liu (1984).

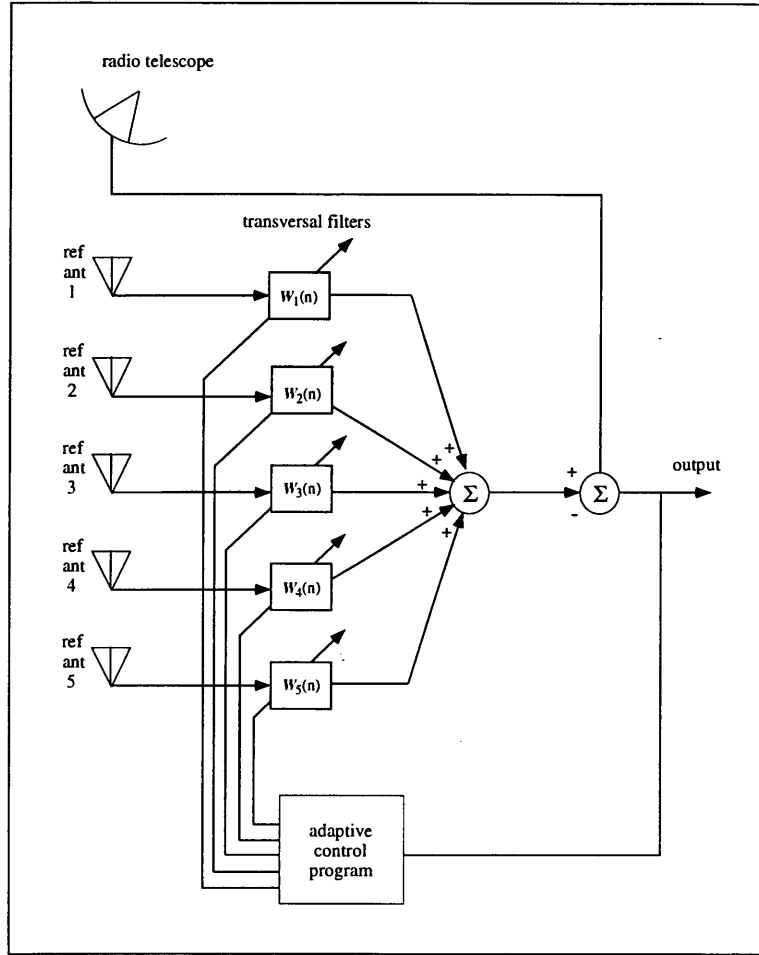


Figure 10 Block diagram of the temporal-spatial interference canceler.

In the digital implementation of an adaptive filter, there are two sources of quantization error: *analog-to-digital (A/D) conversion* and *finite word-length arithmetic*. Analog-to-Digital conversion, using fine quantization levels, results in the generation of white noise with zero mean and a variance determined by the quantizer step size, $\delta = 2^{-b}$ where b is the number of digital bits used to represent a given quantity,

$$\sigma_q^2 = \int_{-\delta/2}^{+\delta/2} \frac{1}{\delta} \eta^2 d\eta = \frac{2^{-2b}}{12} \quad (32)$$

and it is assumed that the quantizer input is properly scaled to lie in the interval

(-1, +1). The finite word-length requires that the adaptive filter be numerically stable, i.e. deviations resulting from the finite-precision arithmetic are bounded. A stable Infinite Impulse Response (IIR) type filter can become unstable with quantized coefficients. Finite Impulse Response (FIR) type filters such as the transversal filter are stable by definition and the quantization effects degrade the performance to some extent.

The quantization errors generated in the digital implementation of the adaptive interference canceler arise from several sources: 1) quantization of the reference channel 2) quantization of the primary channel, 3) quantization of the tap-weight vector, and 4) roundoff of the transversal filter output. Assuming that the step size parameter, μ , is small, and that the quantization of the data and the filter tap-weight coefficients are statistically the same, Caraiscos and Liu show that the total output mean-squared error of the finite-precision algorithm has the following steady-state structure for fixed-point calculations,

$$E [\mathbf{e}_{total}^2(n)] = \xi_{min} + \mu \xi_{min} tr[R(n)] + \frac{L\sigma_q^2}{2a^2\mu} + \frac{1}{a^2} (|W_{opt}(n)|^2 + 1)\sigma_q^2 \quad (33)$$

where ξ_{min} is the minimum mean-squared error, L is the number of tap weights, and a is a scaling constant. The first term is the mean-squared error of the optimal Wiener filter in the presence of only the system noise, $m_p(n)$, and $m_x(n)$. The second term is due to the misadjustment of the infinite-precision LMS algorithm from the Wiener solution, and is proportional to μ (see Section 3.4). The third term arises because of the quantized tap weight vector and is inversely proportional to μ . The fourth term is a result of the quantized reference input and the quantized transversal filter roundoff, and to first order, is independent of μ . *The simulation results presented in this report do not include the quantization errors, which are hardware dependent.* A trade-off in the value of μ is implied here. Such errors will be analyzed during the prototype phase of the adaptive interference canceling project.

3.9 Estimated Performance of the Adaptive Canceler

The performance of the adaptive interference cancellation system was estimated for the following radio telescopes: 1) the Green Bank 140 foot telescope operating at 100 MHz and 1 GHz, 2) the Green Bank Telescope (GBT) operating at 100 MHz and 1 GHz, 3) a VLA antenna operating at 1 GHz, and 4) the Arecibo 1000 foot telescope operating at 100 MHz and 1 GHz. Details are presented in the Appendix.

4.0 Simulations of a Multiple-Reference Interference Canceler

We present here details pertaining to the simulations of a multiple reference interference canceling system. The simulations were performed to identify the trade-offs involved in the design of the canceler. We give a brief description of the simulation software and platform, followed by a description of the canceler under investigation and a summary of the typical input signal characteristics. Next, the simulator is used to gauge the overall performance of the canceler with nominal values chosen for the system parameters. Finally, we investigate the behavior of the canceler as a function of adaptation step size, the number of reference channels, and the primary and reference INR.

4.1 Simulator and Platform

The software package used throughout these simulations is Matlab Version 4.2c, a product of The Math Works Inc., Natick, MA. Matlab is a powerful, comprehensive, and easy-to-use interactive environment, integrating technical computations with graphical visulation. The program was run at the University of Virginia on a SPARCstation-20, operating at 60 MHz, and with 256 MB of RAM. With the typical load average of between 3 and 4, the average runtime was approximately 3 hours for 1000 block averages of data (1 block \equiv 2000 data samples).

4.2 Description of Adaptive Canceler System and Input Signals

A block diagram for the basic multiple reference interference canceler under investigation is shown in Fig. 7, and described in Section 3.5. There are four reference inputs (unless otherwise noted) and a single primary input. We assume that the inputs are from radiometers and are downconverted to a 1.0 MHz baseband where the signal processing takes place. The adjustable filters in the reference channels are nine-tap transversal filters, with the tap weights are controlled by the LMS algorithm. Nine taps were chosen primarily because it emulates our digital filter prototype. The simulations have indicated that less than nine taps will cause degradation in the performance over the full 1 MHz band.

Figure 11 shows the input signals for the primary channel and two of the four reference channels. The abscissa of each graph is the baseband frequency in kilohertz and the ordinate shows relative power in decibels. There are three frequency-modulated interference signals (modulated with random audio tones) in both the primary and reference channels, one at 300, 550, and 800 kHz. White noise is also included in each channel to represent the system noise temperatures. The characteristics of these signals are shown in Table I. There is also a narrow band test signal, located at 300 kHz, with a power level that is 15 dB below the interference power level at that frequency.

Table I Interference signals in the primary and reference channels and estimated canceler performance.

Interference Signal in Baseband [kHz]	Bandwidth [kHz]	INR_{pri} [dB]	$INR_{ref 1 \& 2}$ [dB]	Interference Attenuation [dB]	Residual Noise [%]
300	100	30	37	74	20.0
550	100	22	37	74	3.2
800	25	22	37	74	3.2

4.3 Overall Canceler Performance

The adaptation process was initiated and the LMS algorithm, with step parameter $\mu = 0.00015$, was allowed sufficient time to converge to an optimal solution; the results for 2000 samples (1 block) are displayed in Fig. 12. For comparison, Fig. 12 also contains the perfect interference-free solution which contains only the white noise component. The statistics of the two waveforms are highly correlated in frequency as one would expect if the cancellation is good since the random variables are the same for both cases. Overall, the interference is reduced substantially and the test signal at 300 kHz is visible above the noise floor.

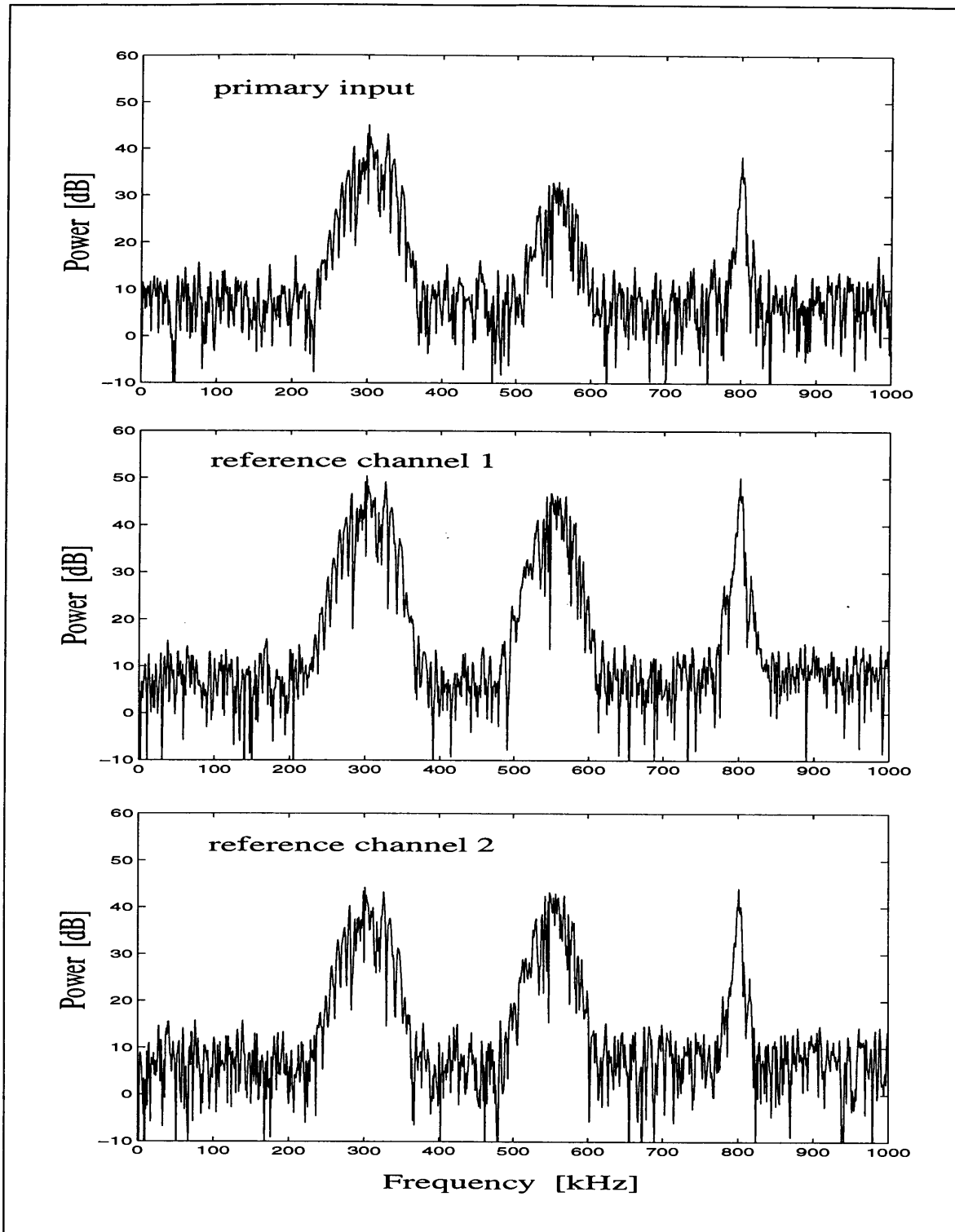


Figure 11 Primary and reference channel (only two shown here) input signals to the four channel adaptive interference canceler. Characteristics of the signals are given in Table I.

Since the $INR_{ref}(z)$ is finite, it is expected that the three interference signals will not be canceled completely, and a residual noise component will remain. The interference attenuation is approximately 74 dB for each interference signal. The residual noise, although frequency dependent, will not affect the noise RMS value, but it will affect the baseline structure at the frequency where the interference is located. Upon comparing the $INR_{ref}(z) / INR_{pri}(z)$ ratio shown in Table I with the graph of Fig. 6, the residual will be on the order of 20 percent for the 300 kHz signal and about 3 percent for the signals at 550 and 800 kHz. Figure 13 shows the canceler output after averaging over 4000 blocks of data. Again, the perfect interference-free solution is included for comparison. The residual noise at 550 and 800 kHz have nearly vanished and the noise RMS value is the same as the in the idealized output. As expected, the residual near 300 kHz is most apparent (maximum about 0.8 dB), manifesting itself as a double sloping baseline, which follows the curve in Fig. 6. The test signal that was 15 dB below the interference power level is now 14 dB above the noise floor. The notch filter phenomenon is present at 800 kHz due to the narrow bandwidth of the interference there and the choice of μ . (see Section 3.6). These results form a framework for the investigations that follow.

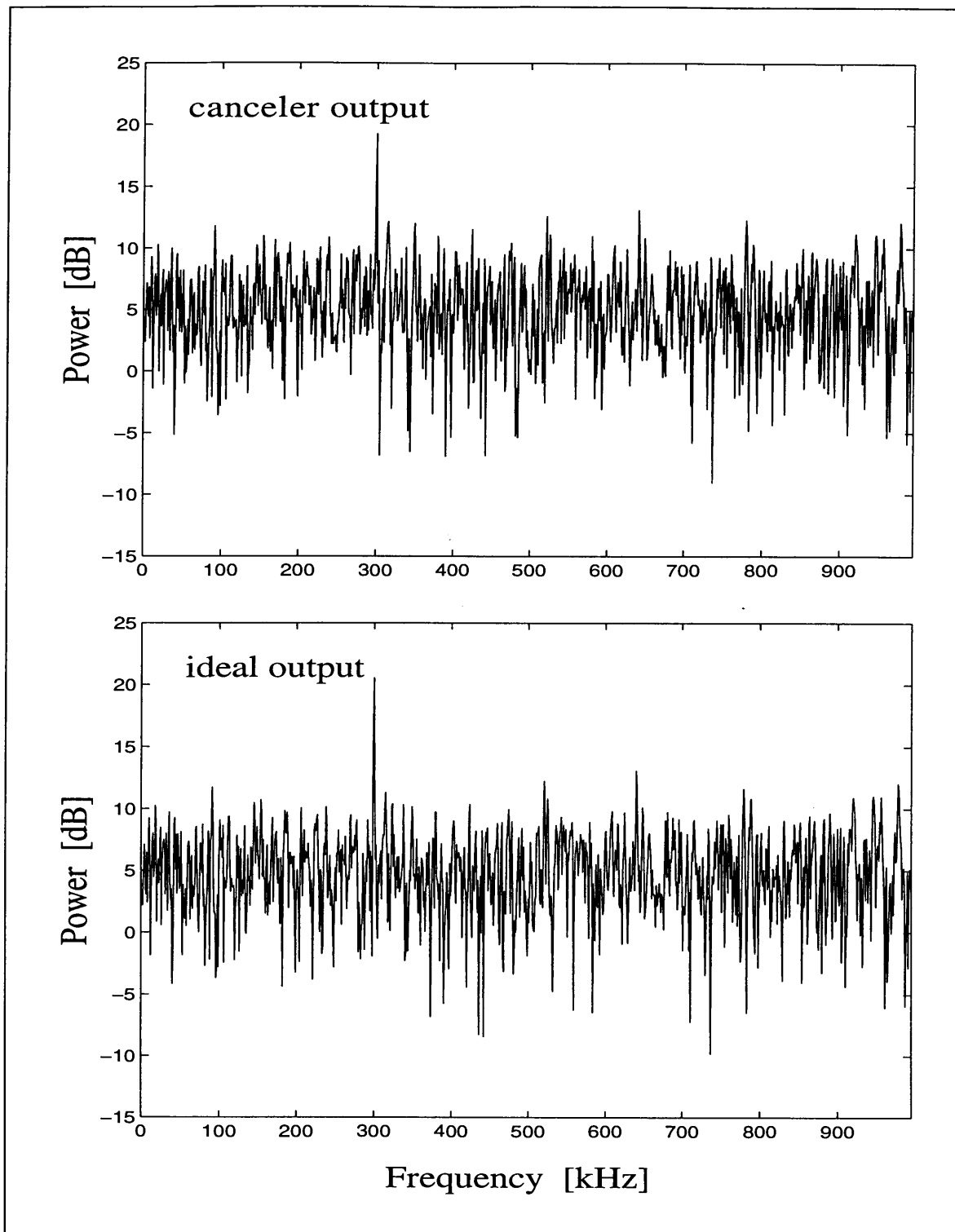


Figure 12 Simulation of a four channel adaptive canceler after convergence of the LMS algorithm. Data represents 2000 samples. The perfect interference-free solution is shown below.

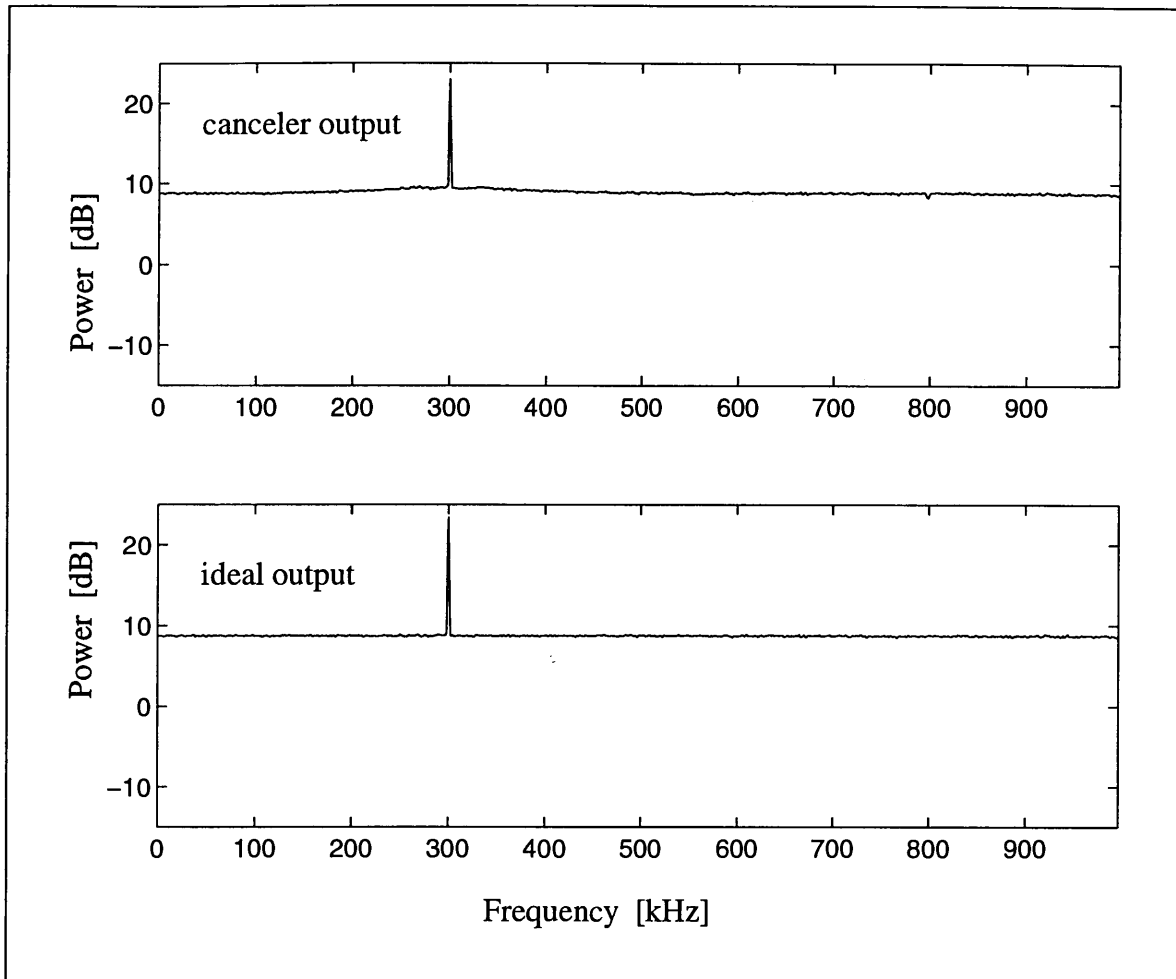


Figure 13 Simulation of a four reference channel adaptive canceler after 4000 block average of the output data. The perfect interference-free solution is shown below.

4.4 Investigation #1: Performance vs. Adaptation Step Size

With the canceler system as described in Section 4.2, we used the simulator to examine the effects of the step size parameter, μ . Figure 14 shows the averaged canceler output data for three values of μ . The smallest value, $\mu = 0.000005$, yields fair performance, yet the baseline contains some structure due to the very slow adaptation time. The notch filter phenomenon is not present in the output when μ is relatively small. *As described in Section 3.8, a small value of μ can result in a large added noise component due to the quantization of the transversal filter tap-weights. This component, which can be significant, is not analyzed in these simulations.*

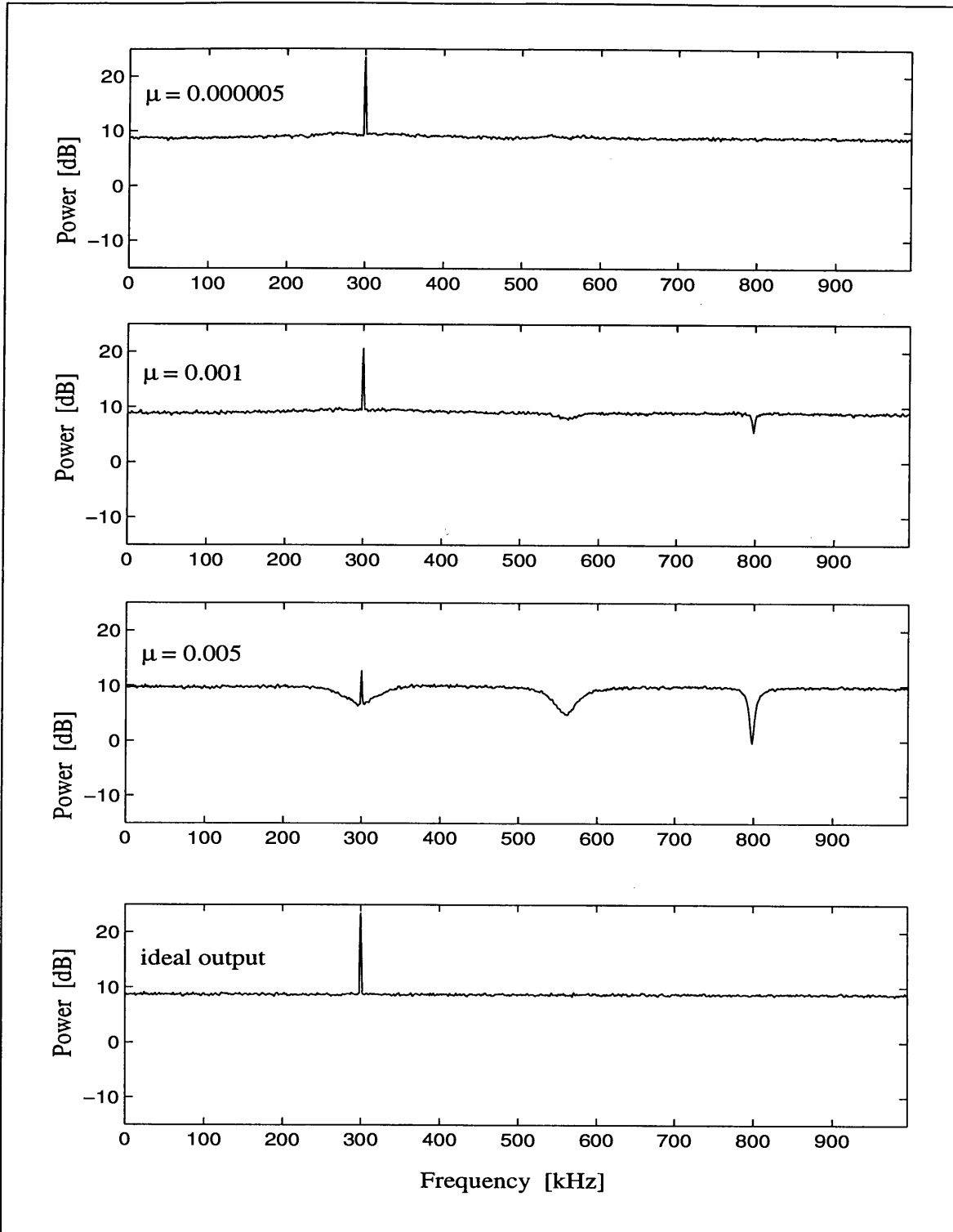


Figure 14 Averaged output of the four reference channel adaptive canceller for three values of LMS algorithm step size parameter μ . The perfect interference-free output is shown below.

As shown in Fig. 14, the adaptation process resulting from larger values of μ suffer from two problems: 1) the notch bandwidth, as described by equation (31), is very large thus causing significant distortion in the passband, and 2) the misadjustment becomes large causing a jitter-type movement toward and around the minimum in the error performance surface as described by equation (25). This jitter movement results in increased noise at the canceler output. Equation (25) also indicates that the misadjustment is a function of the reference signal power (proportional to the trace of the input correlation matrix). *In order to maintain proper operation over a wide dynamic range of interference signals powers, it is recommended that the value of μ be fixed and either an automatic gain control be used on all reference channels, or after A/D conversion the reference channels should be scaled by a factor inversely proportional to the interference power in that channel.*

4.5 Investigation #2: Performance vs. Number of Reference Channels

We examine the performance of the canceler as a function of the number of reference channels having interference signals and noise spectrum as outlined in Table I. Averaged canceler output data is shown in Fig. 15 for the case of one, two, and four reference channels. The perfect interference-free solution is also included for comparison. A system having only one reference channel shows uncanceled interference components at all three interference frequencies. These residuals are due to the transversal filter being of finite length and therefore a transfer function with enough resolution to cover the entire operating range cannot be formed. Having two reference channels makes a sizable improvement, particularly at 550 and 800 kHz, and going to four reference channels improves the cancellation further to the point where the overall operation is now limited by the interference-to-noise ratios in the primary and reference channels. The notch filter phenomenon is present only when four reference channels are used, which is consistent with the discussion in Section 3.6.

4.6 Investigation #3: Performance vs. Primary Channel Noise Power

Here we investigate the effects of varying the primary channel noise temperature while all of the other parameters are held constant. The canceler input is shown in Fig. 11 and the averaged output for several values for the system temperature are presented in Fig. 16. $INR_{ref}(z)$ is the same as shown in Table I. The graph showing $1 \times T_{sys}$ is the same as that in Fig. 13 and is included here for comparison. For extremely small primary channel system noise temperatures (making $INR_{pri}(z)$ equal to 56, 48, and 48 dB for the 300, 550, and 800 kHz interference signals respectively), the residual noise powers are quite large, as expected from the graph in Fig. 6. The notch filter phenomenon, observable at 800 kHz, is unaffected by the noise power in the primary channel (assuming that a good replica of the interference is present in the reference channels) since it is a function only of μ and the interference signal bandwidth.

4.7 Investigation #4: Performance vs. Reference Channel Noise Power

Now, we alter the interference-to-noise ratio in the reference channels while holding all other system parameters constant. The canceler input is as shown in Fig. 11 and the averaged output data are displayed in Fig. 17. The $INR_{pri}(z)$ is the same as that in Table I. The graph for $INR_{ref}(z) = 37$ dB is the same as that in Fig. 13. The perfect interference-free solution is also included for comparison. When the $INR_{ref}(z)$ is infinite, the cancellation is complete except for evidence of the notch filter phenomenon. As predicted by the curves in Fig. 6, when the $INR_{ref}(z) = 12$ dB, yielding a INR_{ref} / INR_{pri} ratio of -18, -10, and -10 dB for the interference at 300, 550, and 800 kHz respectively, the cancellation is very poor with significant residual noise power and large baseline distortion.

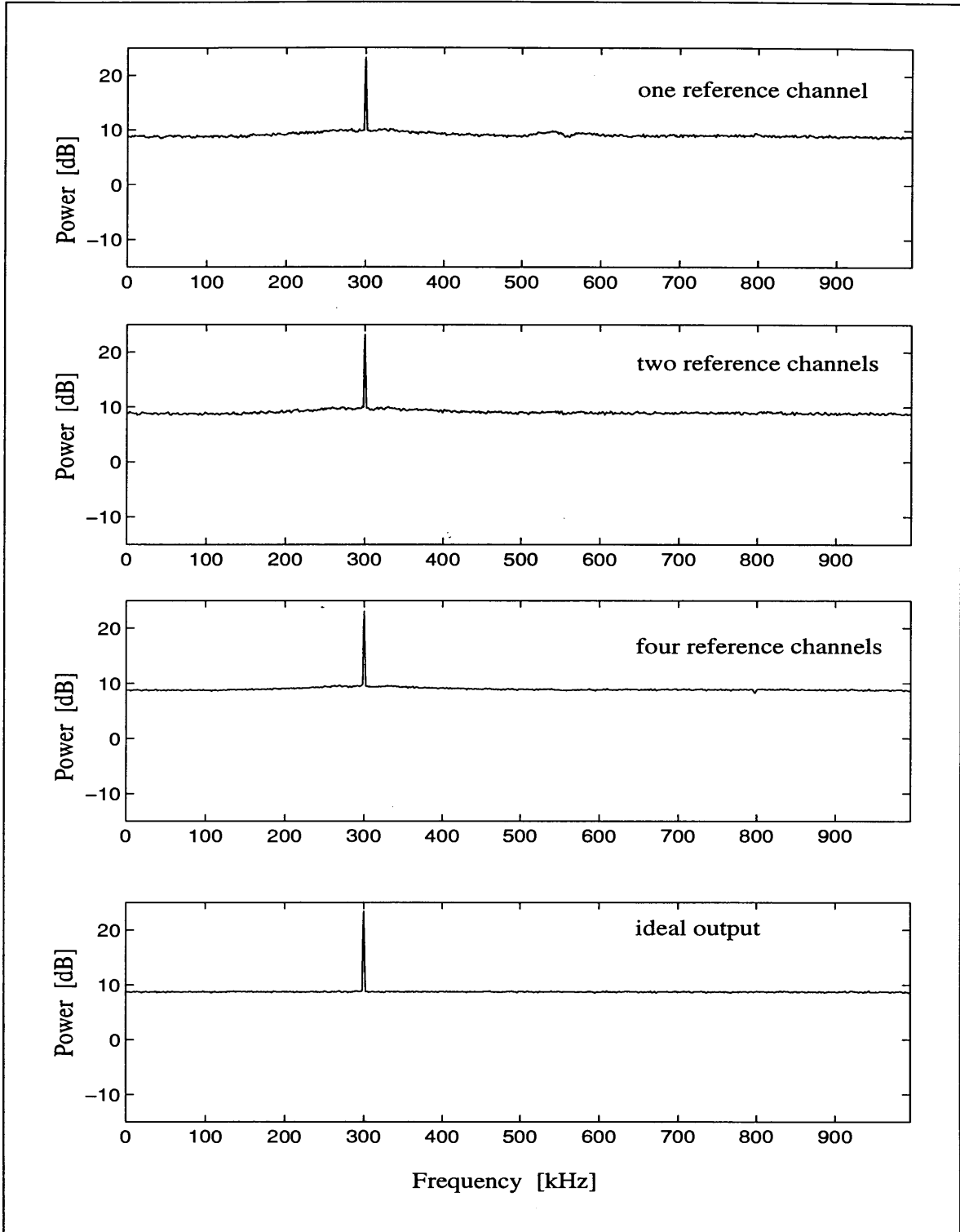


Figure 15 Averaged canceler output data for simulated adaptive interference cancelers having one, two, and four reference channels. Canceler input is described in Fig. 11 and Table I.

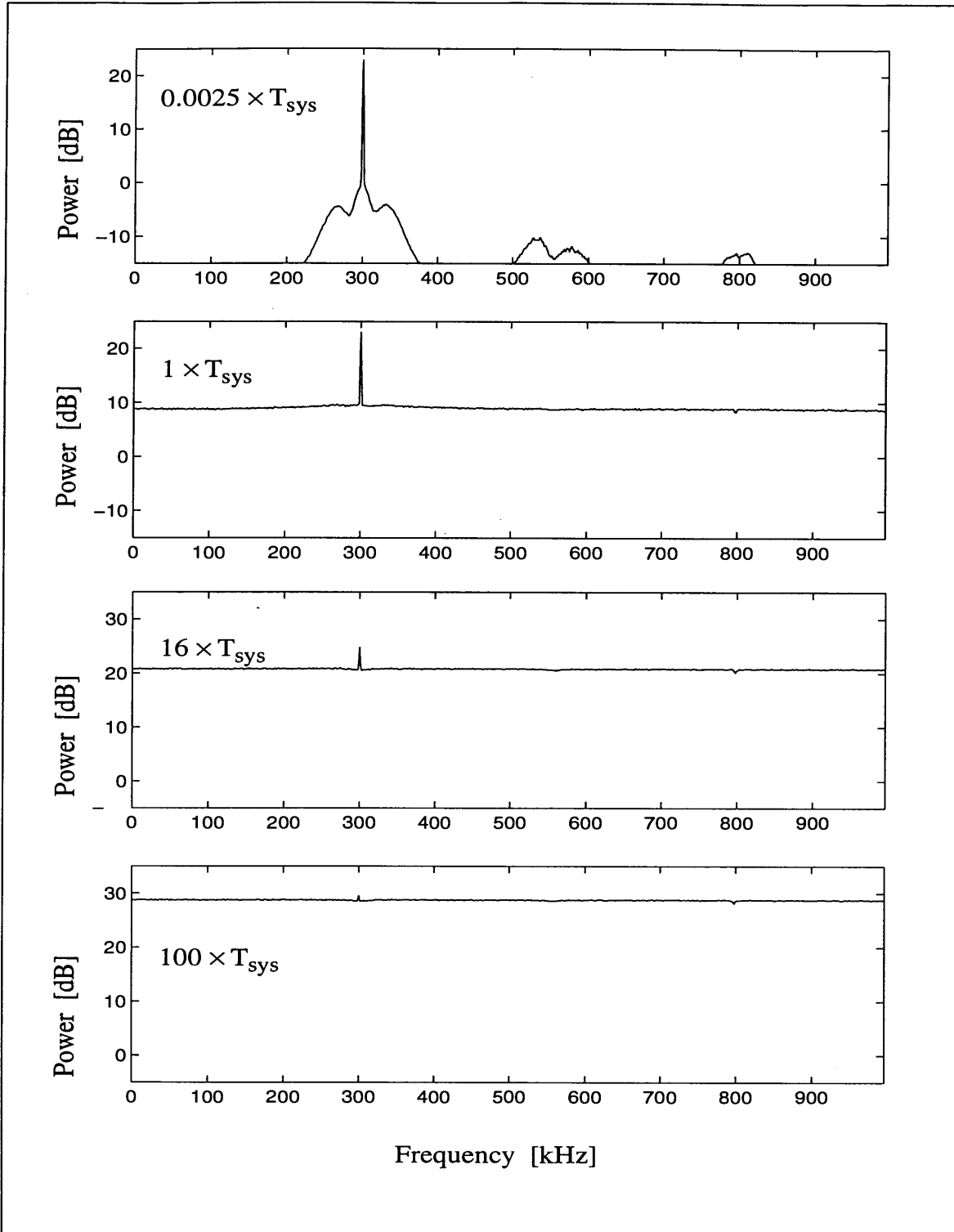


Figure 16 Averaged output for the simulated four reference channel interference canceler with four possible system temperatures in the primary channel.

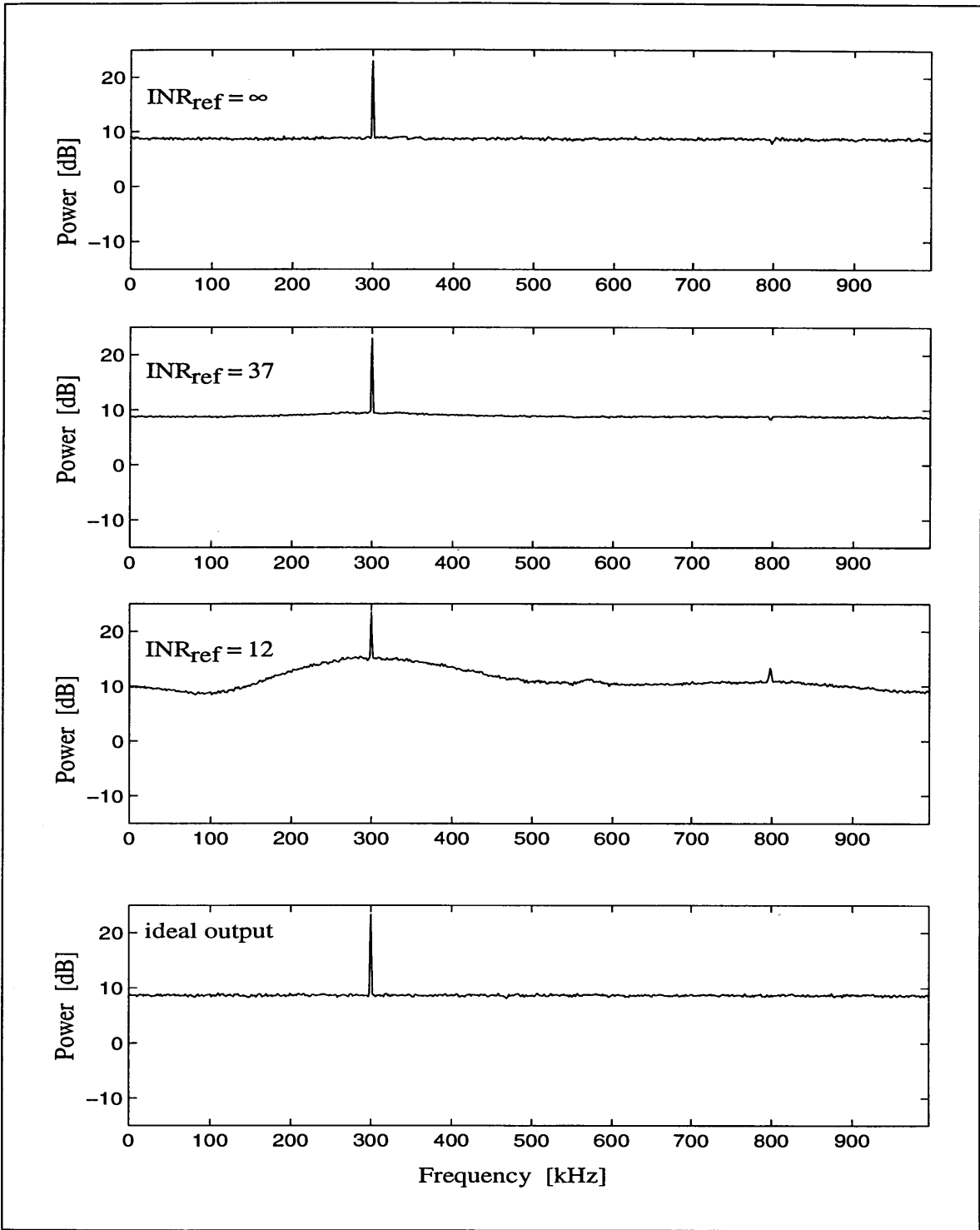


Figure 17 Simulation of a four reference channel adaptive interference canceler. The parameter under investigation is the INR_{ref} . The perfect interference-free output is shown below.

5.0 Conclusions

We have demonstrated that adaptive interference cancellation can be used successfully for radio astronomy applications on a variety of radio telescopes only when the adaptive approach is properly implemented and its limitations well understood. In the design of adaptive canceler systems, the following points must be considered:

1. Minimizing the total output power of the adaptive canceler minimizes the output interference power, yet has no effect on the desired signal.
2. The desired signal must not be present in the reference channel or a portion of it too will be canceled.
3. If the reference input is completely uncorrelated with the primary input, the algorithm will turn off the transversal filter and the output noise power of the canceler will not increase.
4. A suitable delay must be inserted into the primary channel so that a noncausal, two-sided filter can be formed in the reference channel.
5. The optimum transversal filter tap-weight vector is independent of the astronomical source spectrum and the primary system noise spectrum.
6. A large value of reference channel INR is necessary for adequate interference cancellation.
7. A large ratio of reference channel INR to primary channel INR is essential for minimizing the noise added by the canceler.
8. The number of reference channels must be greater than or equal to the number of interference signals present in the passband.
9. Under certain conditions, a notch filter can occur in response to a fixed frequency interference waveform present in the reference channels and will cause cancellation of all primary channel input components at that frequency as well as at adjacent frequencies.
10. Quantization effects must be understood prior to canceler hardware design. The interference-to-noise ratios at the front-end of the radiometers must be the limiting factor governing canceler performance.
11. The value of step size should be adjustable in accordance with the power level of the interference present in the reference channel. Otherwise, an Automatic Gain Control (AGC) should be used at the input of each reference channel or the reference channel power should be scaled upon A/D conversion.
12. The minimum number of tap weights used with the transversal filter depends on the bandwidth of the adaptive canceler.

Appendix

Estimate of Adaptive Interference Canceler Performance on Several Radio Telescopes

The effectiveness of the adaptive interference canceling system for reducing interference during astronomical observations is estimated. Four radio telescopes are considered: 1) the Green Bank 140 foot telescope operating at 100 MHz and 1 GHz, 2) the Green Bank Telescope (GBT) operating at 100 MHz and 1 GHz, 3) a VLA antenna operating at 1 GHz, and 4) the Arecibo 1000 foot telescope operating at 100 MHz and 1 GHz. The performance will be estimated from rough calculations of $INR_{ref}(z)$ and $INR_{pri}(z)$ for each of the canceler-telescope systems. We assume that the interference levels at both frequencies are -97.5 dBm, which is based on measurements made at 93.5 MHz in Green Bank (see Fig. 1).

The following assumptions are made in order to simplify the calculations: All of the radio telescopes are symmetrical paraboloids and that the interference is in the far-field of the telescope radiation pattern. $T_{sys P}$ at 100 MHz and 1 GHz depends on the radiometers used with each telescope, but is assumed to be independent of elevation angle.

The type of reference antenna chosen for the canceler will depend on the operating frequency. For 100 MHz operation, a dual-polarized, 5-element yagi antenna is chosen so that a beam with 10 dB of gain over an isotrope is pointed along the horizon in the direction of the interference source, located at azimuth angle α_{ψ} . $T_{sys X}$ at 100 MHz is taken to be 750 K for ambient temperature operation. Similarly, at 1 GHz, a dual-polarized horn antenna is chosen so that a beam with 20 dB of gain over an isotrope is pointed along the horizon in the direction of the interference source at α_{ψ} . $T_{sys X}$ at 1 GHz is taken to be 300 K. In both cases, knowledge of the direction of the interference is assumed in order to simplify the calculations.

The telescope main beam gain, G_{main} , is estimated by the well-known equation (Stutzman et al., 1981),

$$G_{main} \approx 10 \log \left[\kappa \left(\frac{\pi D}{\lambda} \right)^2 \right] \quad [dB] \quad (\text{A } 1)$$

where D is the aperture diameter [meters], λ is the operating wavelength [meters], and κ , the aperture efficiency, is taken to be 60 percent.

The half power beamwidth, $2\theta_0$, is calculated using the following formula (Stutzman et al., 1981),

$$2 \cdot \theta_0 \approx 74.48 \frac{\lambda}{D} \quad [degrees] \quad (\text{A } 2)$$

The sidelobe gain along at horizon, $G_{side}(\beta)$, is estimated using the following formula (Korvin et al., 1971),

$$G_{side}(\beta) = 10 \log \left[1 + \left(\frac{90^\circ - \beta}{\theta_0} \right)^{2.5} \right]^{-1} \quad [dB] \quad (\text{A } 3)$$

where β is the elevation angle [degrees] at which the telescope is pointing. We assume here that the telescope is pointed in the direction (α_{ψ}, β) . This assumption is made only to establish a frame of reference.

The noise powers at both the primary and reference channel receiver front-ends are calculated from the respective system temperatures as

$$P_{noise} = 10 \log (kBT \cdot 10^3) \quad [dBm] \quad (\text{A } 4)$$

where k is Boltzmann's constant, $1.38 \times 10^{-23} \text{ W Hz}^{-1} \text{ K}^{-1}$, B is the bandwidth [Hz], and T is the noise temperature [kelvins].

Estimates of the canceler performance for the four telescope systems are presented below.

Green Bank 140 Foot - 100 MHz

Interference:

Power Level at Antenna [dBm]: -97.5
 Bandwidth [kHz]: 100

Telescope:

Aperture Diameter [meters]: 43
 Main Beam Gain [dB]: 30.9
 Main Beam Half Width [deg]: 2.6
 System Temp. [K]: 750
 Noise Power [dBm]: -119.9

Horizon Sidelobe Gain:

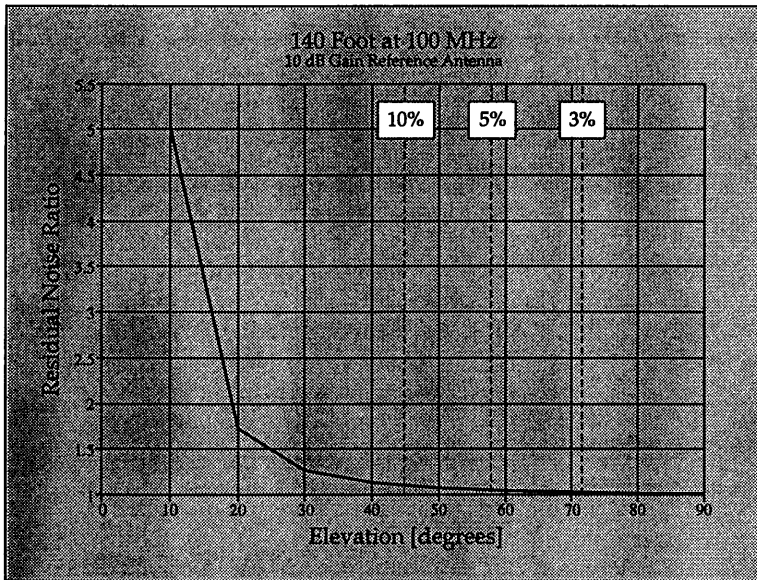
Elev. [deg], Gain [dB]: 90 -7.6
 50 -1.3

Interference-to-Noise:

Elev. [deg], INR_{pri} [dB]: 90 14.7
 50 21.1

Reference:

Antenna Gain [dB]: 10
 System Temperature [K]: 750
 Noise Power [dBm]: -119.9
 INR_{ref} [dB]: 32.4



PERFORMANCE:

Interference Attenuation [dB]: 64.7

Residual Noise Ratio:

Elev. [deg], Ratio [dB]: 90 1.017
 50 1.075

Green Bank 140 Foot - 1 GHz

Interference:

Power Level at Antenna [dBm]: -97.5
 Bandwidth [kHz]: 100

Telescope:

Aperture Diameter [meters]: 43
 Main Beam Gain [dB]: 50.8
 Main Beam Half Width [deg]: 0.26
 System Temp. [K]: 20
 Noise Power [dBm]: -135.6

Horizon Sidelobe Gain:

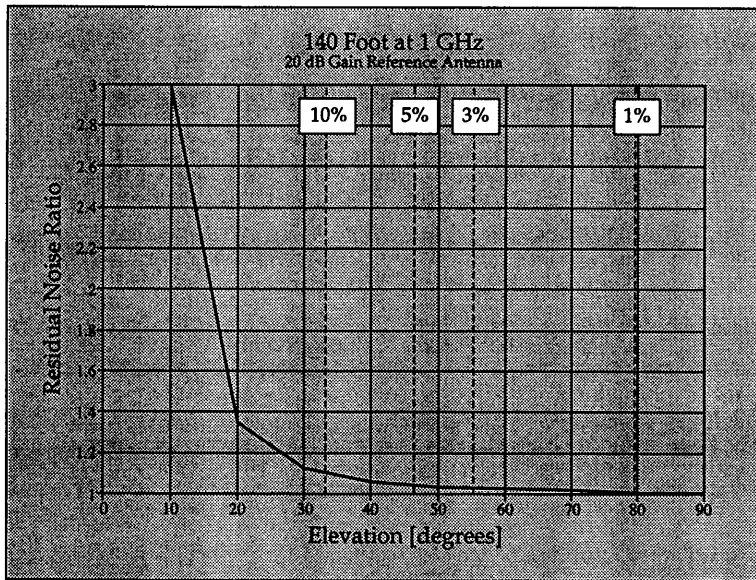
Elev. [deg], Gain [dB]: 90 -12.6
 50 -6.3

Interference-to-Noise:

Elev. [deg], INR_{pri} [dB]: 90 25.4
 50 31.8

Reference:

Antenna Gain [dB]: 20
 System Temperature [K]: 300
 Noise Power [dBm]: -123.8
 INR_{ref} [dB]: 46.3



PERFORMANCE:

Interference Attenuation [dB]: 92.7
 Residual Noise Ratio:
 Elev. [deg], Ratio [dB]: 90 1.0082
 50 1.0355

GBT - 100 MHz

Interference:

Power Level at Antenna [dBm]: -97.5
 Bandwidth [kHz]: 100

Telescope:

Aperture Diameter [meters]: 100
 Main Beam Gain [dB]: 38.2
 Main Beam Half Width [deg]: 1.1
 System Temp. [K]: 300
 Noise Power [dBm]: -123.8

Horizon Sidelobe Gain:

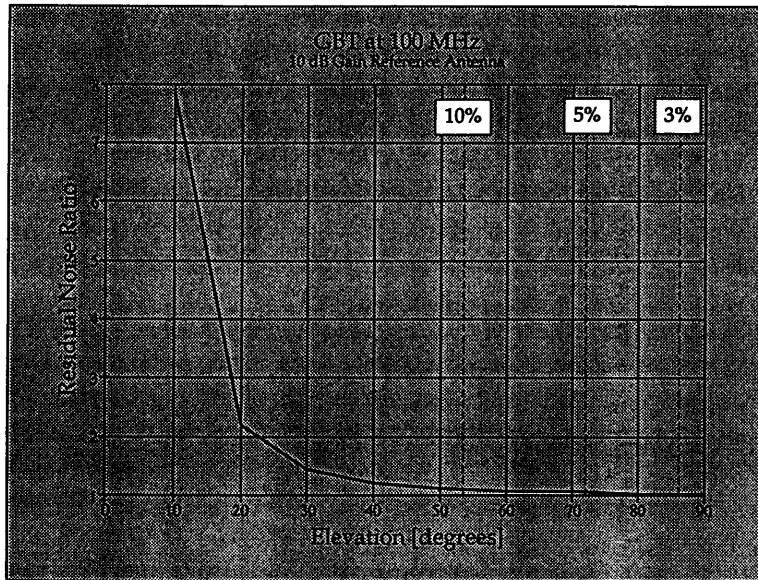
Elev. [deg], Gain [dB]:	90	-9.5
	50	-3.1

Interference-to-Noise:

Elev. [deg], INR_{pri} [dB]:	90	16.9
	50	23.2

Reference:

Antenna Gain [dB]: 10
 System Temperature [K]: 750
 Noise Power [dBm]: -119.9
 INR_{ref} [dB]: 32.4



PERFORMANCE:

Interference Attenuation [dB]: 64.7
 Residual Noise Ratio:
 Elev. [deg], Ratio [dB]:

90	1.0282
50	1.12275

GBT - 1 GHz

Interference:

Power Level at Antenna [dBm]: -97.5
 Bandwidth [kHz]: 100

Telescope:

Aperture Diameter [meters]: 100
 Main Beam Gain [dB]: 58.2
 Main Beam Half Width [deg]: 0.11
 System Temp. [K]: 15
 Noise Power [dBm]: -136.84

Horizon Sidelobe Gain:

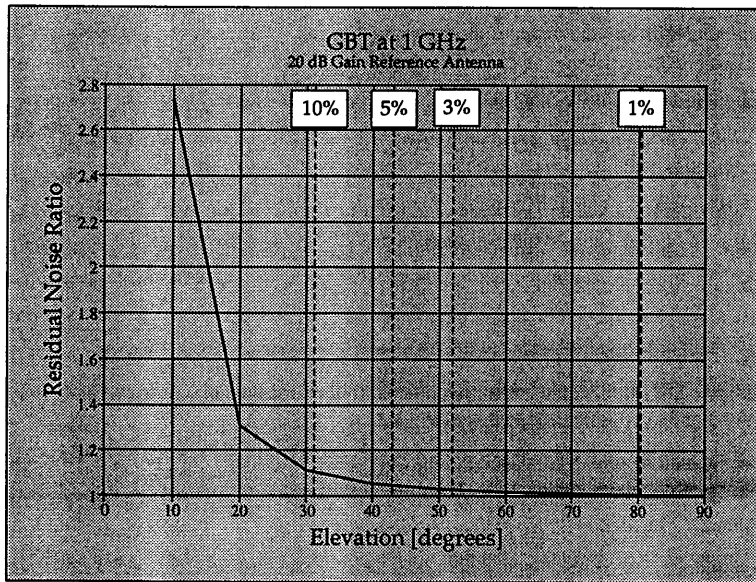
Elev. [deg], Gain [dB]: 90 -14.5
 50 - 8.1

Interference-to-Noise:

Elev. [deg], INR_{pri} [dB]: 90 25.4
 50 31.8

Reference:

Antenna Gain [dB]: 20
 System Temperature [K]: 300
 Noise Power [dBm]: -123.8
 INR_{ref} [dB]: 46.3



PERFORMANCE:

Interference Attenuation [dB]: 92.7
 Residual Noise Ratio:
 Elev. [deg], Ratio [dB]: 90 1.00714
 50 1.03106

VLA - 1 GHz

Interference:

Power Level at Antenna [dBm]: -97.5
 Bandwidth [kHz]: 100

Telescope:

Aperture Diameter [meters]: 23
 Main Beam Gain [dB]: 45.4
 Main Beam Half Width [deg]: 0.49
 System Temp. [K]: 50
 Noise Power [dBm]: -131.6

Horizon Sidelobe Gain:

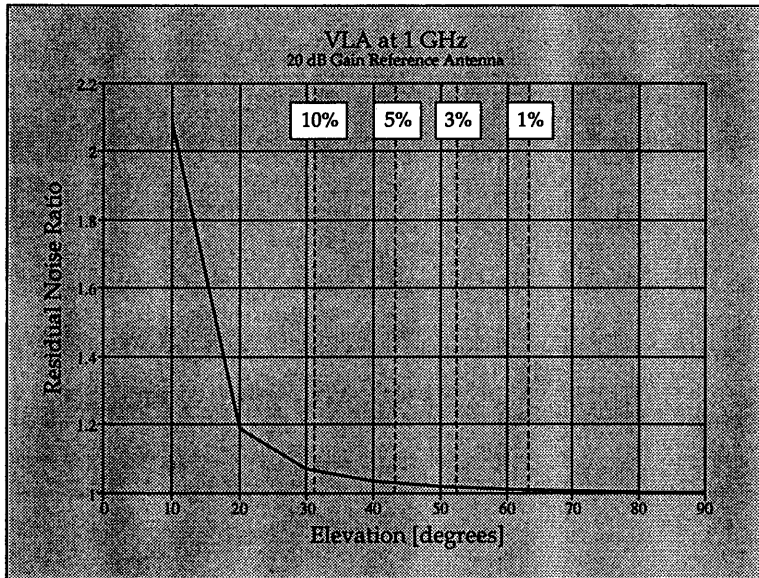
Elev. [deg], Gain [dB]: 90 -11.3
 50 - 4.9

Interference-to-Noise:

Elev. [deg], INR_{pri} [dB]: 90 22.8
 50 29.2

Reference:

Antenna Gain [dB]: 20
 System Temperature [K]: 300
 Noise Power [dBm]: -123.8
 INR_{ref} [dB]: 46.3



PERFORMANCE:

Interference Attenuation [dB]: 92.7
 Residual Noise Ratio:
 Elev. [deg], Ratio [dB]: 90 1.00447
 50 1.01943

Arecibo - 100 MHz

Interference:

Power Level at Antenna [dBm]: -97.5
 Bandwidth [kHz]: 100

Telescope:

Aperture Diameter [meters]: 305
 Main Beam Gain [dB]: 47.9
 Main Beam Half Width [deg]: 0.37
 System Temp. [K]: 750
 Noise Power [dBm]: -119.9

Horizon Sidelobe Gain:

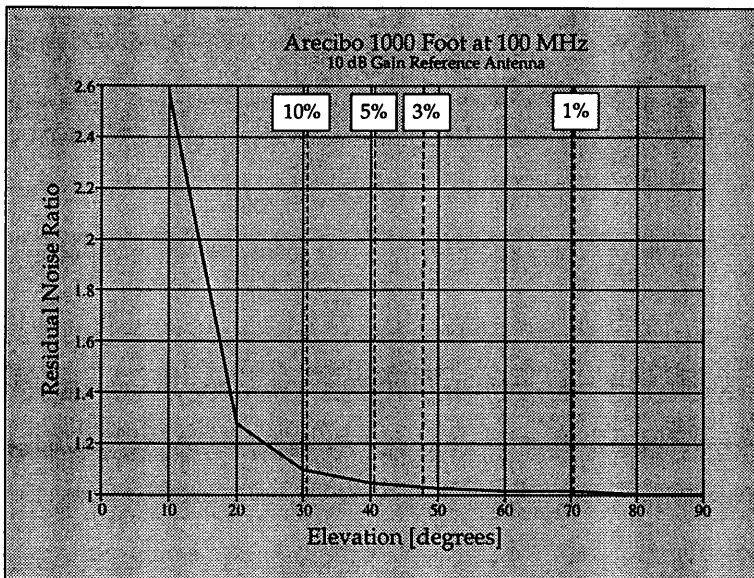
Elev. [deg], Gain [dB]:	90	-11.9
	50	- 5.5

Interference-to-Noise:

Elev. [deg], INR_{pri} [dB]:	90	10.4
	50	16.8

Reference:

Antenna Gain [dB]: 10
 System Temperature [K]: 750
 Noise Power [dBm]: -119.9
 INR_{ref} [dB]: 32.4



PERFORMANCE:

Interference Attenuation [dB]: 64.7
 Residual Noise Ratio:
 Elev. [deg], Ratio [dB]: 90 1.00647
 50 1.02812

Arecibo - 1 GHz

Interference:

Power Level at Antenna [dBm]: -97.5
 Bandwidth [kHz]: 100

Telescope:

Aperture Diameter [meters]: 305
 Main Beam Gain [dB]: 67.9
 Main Beam Half Width [deg]: 0.04
 System Temp. [K]: 50
 Noise Power [dBm]: -131.6

Horizon Sidelobe Gain:

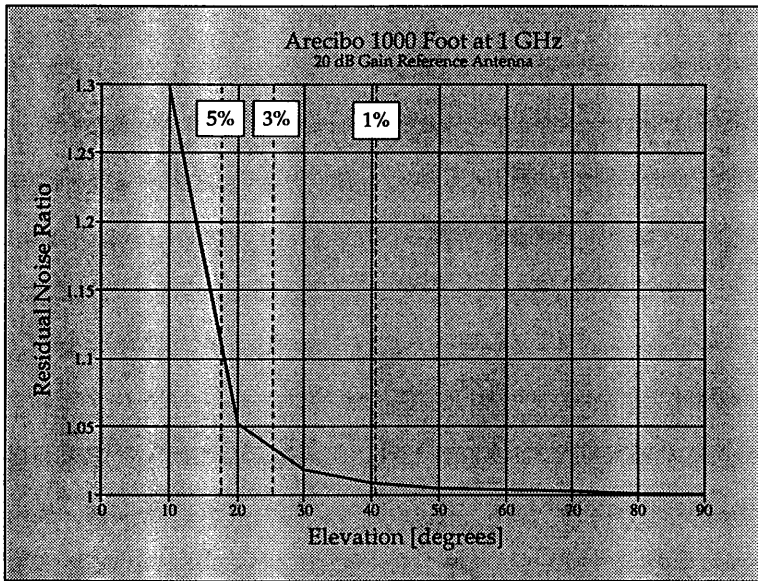
Elev. [deg], Gain [dB]:	90	-16.9
	50	-10.5

Interference-to-Noise:

Elev. [deg], INR_{pri} [dB]:	90	17.2
	50	23.6

Reference:

Antenna Gain [dB]: 20
 System Temperature [K]: 300
 Noise Power [dBm]: -123.8
 INR_{ref} [dB]: 46.3



PERFORMANCE:

Interference Attenuation [dB]: 92.7
 Residual Noise Ratio:

Elev. [deg], Ratio [dB]:	90	1.00123
	50	1.00534

List of Symbols

ables and Constants

A	Amplitude of sinusoidal signal
a	Scaling factor for fixed-point arithmetic operations
b	Number of bits used during quantizing
B	Bandwidth
B_{notch}	Bandwidth of adaptive notch filter
D	Telescope aperture diameter
$\nabla(n)$	Gradient estimate
$F_{ij}(z)$	Transfer functions from interference sources to reference shann
$G_i(z)$	Transfer functions from interference sources to primary input
G_{main}	Telescope main beam gain
$G_{side}(\theta)$	Telescope sidelobe gain
$H(z)$	Transfer function between interference source & reference inpu
$h(n)$	Impulse response of $H(z)$
IA	Interference attenuation
INR_{pri}	Interference-to-noise ratio in the primary channel
INR_{ref}	Interference-to-noise ratio in the reference channel
$i_p(n)$	Interference entering primary antenna
$i_x(n)$	Interference entering reference antenna
k	Boltzmann's constant, $1.38 \times 10^{-23} \text{ W Hz}^{-1} \text{ K}^{-1}$
L	Number of tap weights
M_{ADJ}	Misadjustment
$m_p(n)$	Noise component from $T_{sys P}$
$m_x(n)$	Noise component from $T_{sys X}$
n	Discrete time sequence
P_{noise}	Noise power in bandwidth B
$p(n)$	Primary channel input
$R(z)$	Input correlation matrix
RNR	Residual noise ration

List of Symbols

-- continued --

$s(n)$	Desired signal
SIR	Signal-to-interference ratio
T	Noise temperature
$T_{sys P}$	Primary channel system noise temperature
$T_{sys X}$	Reference channel system noise temperature
$W(n)$	Tap weight vector which includes the set of $w_i(n)$
$w_i(n)$	Transversal filter tap weight
W_{opt}	Vector containing the set of optimum tap weights
$W_{opt}(z)$	Optimum filter transfer function (z-transform of W_{opt})
$X(n)$	Vector containing delayed versions of the reference input
$x(n)$	Reference channel input (also transversal filter input)
$y(n)$	Transversal filter output
z^{-1}	Unit delay
α_ψ	Azimuth angle of interference
β	Elevation angle
δ	Quantizer step size
$\varepsilon(n)$	Interference canceler output and error feedback signal
θ_0	1/2 the beamwidth at the half-power points
κ	Aperture efficiency
λ	wavelength
μ	Step size parameter
ξ	Error performance surface or mean-squared error
ξ_{min}	Minimum mean-squared error
π	pi, 3.14159
σ_q^2	Variance of the white noise due to quantization
Φ_{ii}	Signal power spectrum
Φ_{ij}	Cross power spectrum
$\Phi_{io io}$	Interference power spectrum at the canceler output

List of Symbols

-- continued --

ϕ_{ii}	Auto-correlation
ϕ_{ij}	Cross-correlation
ψ_i	Interference source

Mathematical Operations

$E[]$	Expectation operator
$tr[]$	Matrix trace operator
T	Matrix transposition
$*$	Complex conjugation

Bibliography

- Bullock, S., (1990). "High Frequency Adaptive Filter," *Microwave J.*, vol. 33, Sept., pp. 97+.
- Caraiscos, C. and B. Liu (1984). "A Roundoff Error Analysis of the LMS Algorithm," *IEEE Trans. on Acoust. Speech & Signal Process.*, vol. ASSP-32, pp. 34-41.
- Erickson, W. (1982). "Excision of Terrestrial Interference from Meter-Wavelength Radio Data," *Proc. of the Interference Identification and Excision Workshop*, Green Bank, WV, National Radio Astronomy Observatory, pp. 78-90.
- Fisher, J. R. (1982). "An Impulse Noise Suppress and Other Thoughts on Interference Reduction," *Proc. of the Interference Identification and Excision Workshop*, Green Bank, WV, National Radio Astronomy Observatory, pp. 100-111.
- Fleisch, D. A and G.C. Pieters, (1991). "The ACT Programmable Transversal Filter," *Microwave J.*, vol. 34, May, pp. 284+.
- Gerard, E. (1982). "A Radar Blanker at Stockert Observatory," *Proc. of the Interference Identification and Excision Workshop*, Green Bank, WV, National Radio Astronomy Observatory, p.63.
- Goldberg, L. (1995). "Adaptive-Filtering Developments Extend Noise-Cancellation Applications," *Electronic Design*, vol. 43, Feb. 6, pp. 34+.
- Haykin, S. (1996). Adaptive Filter Theory, 3rd ed., Prentice-Hall, Upper Saddle River, New Jersey.
- Howells, P. W. (1976). "Explorations in Fixed and Adaptive Resolution at GE and SURC," *IEEE Trans. on Antennas and Propag.*, vol. AP-24, Special Issue on Adaptive Antennas, pp. 753-763.
- Korvin, W. and R. W. Kreutel (1971). "Earth Station Radiation Diagram with Respect to Interference Isolation Capability: A Comparative Evaluation," *AIAA Progress in Astronautics & Aeronautics: Communications Satellites for the 70's: Technology*, vol 25, M.I.T. Press, Cambridge, MA. pp. 535-548.
- Lin A. and R Monzello, (1992) "An Interference Cancellation System for EW Applications Using an ACT Device," *Microwave J.*, vol. 35, Feb., pp. 118+.
- Logic Devices Inc. (1995). Digital Signal Processing Databook, Sunnyvale, CA., p. 4-45.
- Moffet, A. (1982). "JPL Work on Superconducting Filters," *Proc. of the Interference Identification and Excision Workshop*, Green Bank, WV, National Radio Astronomy Observatory, pp. 91-95.
- Morton, J. R., K. F. Preston, P. J. Krusic, and L. B. Knight Jr. (1993). "The Proton Hyperfine Interaction in HC_{60} Signature of a Potential Interstellar Fullerene," *Chem. Phys. Lett.*, vol. 204, no. 5, 6, March 26, pp. 481-485.
- Oppenheim, A. V. and R. W. Schaffer, (1989). Discrete-Time Signal Processing, Prentice- Hall, Englewood Cliffs, NJ.

- Schultz, R. B. (1971). Practical Design for Electromagnetic Compatibility, R. F. Ficchi ed., Ch. 6.
- Shin, D. C., and C. L. Nikias (1994). "Adaptive Interference Canceler for Narrowband and Wideband Interferences Using Higher Order Statistics," *IEEE Trans. on Signal Processing*, vol. 42, no. 10, October, pp. 2715-2728.
- Sizemore, W. A. (1991). "National Radio Quiet Zone and the Green Bank RFI Environment," *IAU Colloquium no. 112*, Astronomical Society of the Pacific, pp. 176-180.
- Sondhi, M.N., (1967). "An Adaptive Echo Canceller," *Bell Syst. Tech. J.*, vol 46, pp. 497-511.
- Stutzman, W. L. and G. Thiele (1981). Antenna Theory and Design, John Wiley, New York, sections 8.5 & 8.6.
- Superconducting Technologies Inc. (1994). "Superconducting Filter Screens Cellular Signals," *Microwaves & RF*, vol. 33, Dec., p. 226.
- Widrow B., P. E. Mantey, L. J. Griffiths, and B. B. Goode (1967). "Adaptive Antenna Systems," *Proc. of the IEEE*, vol. 55, no. 12, Dec., pp. 2143-2159.
- Widrow, B., J. R. Glover, J. M. McCool, J. Kaunitz, C. S. Williams, R. H. Hearn, J. R. Zeidler, E. Dong, and R. Goodlin, (1975). "Adaptive Noise Cancelling: Principles and Applications," *Proc. of the IEEE*, vol. 63, no. 12, Dec., pp. 1692-1716
- Widrow, B., and S. Stearns, (1985). Adaptive Signal Processing, Prentice-Hall, Englewood Cliffs, NJ.